Eur. J. Mineral.
2007, **19**, 439–461
Published online August 2007

Fluid evolution from metamorphic peak to exhumation in Himalayan granulitised eclogites, Ama Drime range, southern Tibet

SIMONA FERRANDO[1,*], FRANCO ROLFO[1,2] and BRUNO LOMBARDO[2]

[1] Department of Mineralogical and Petrological Sciences, University of Torino, via Valperga Caluso 35, 10125 Torino, Italy
*Corresponding author, e-mail: simona.ferrando@unito.it
[2] C.N.R., Institute of Geosciences and Georesources, via Valperga Caluso 35, 10125 Torino, Italy

Abstract: A fluid inclusion study has been carried out on granulitised eclogites and associated amphibolite-facies veins from the eastern Himalaya (Ama Drime range, southern Tibet) in order to better characterise the fluid evolution of continental crust involved in Cenozoic subduction and continent-continent collision processes.

Six distinct events of fluid influx have been characterised on the basis of petrographic observations and microthermometric measurements: 1) a high-density - medium-salinity aqueous fluid with CO_2, trapped at the eclogitic peak (metamorphic stage M1); 2) pure CO_2, present at the granulitic stage M2; 3) a low-salinity – low-density aqueous fluid with minor CO_2 in equilibrium with amphibole-bearing LP-M/HT mineral assemblage (stage M4); 4) a low-density aqueo-carbonic fluid responsible of vein formation (stage M5); 5) a subsequent influx of a low-density CO_2-rich fluid; 6) a late influx of very-low salinity aqueous fluid.

Comparing these data with those obtained from other localities of the Himalayas and from other collisional orogens, an internal origin is proposed for eclogitic and granulitic fluids, whereas an origin from the underlying metasediments of the Lesser Himalaya is suggested for the subsequent types of fluid, safe for the meteoric origin proposed for the latest fluid influx.

Key-words: fluid inclusion study, microthermometry, eclogite, vein, Himalaya.

Introduction

The Himalaya is the most promising orogen to study Cenozoic continent-continent collision processes and, also, to characterise the nature and evolution of metamorphic fluids during subduction and exhumation of continental crust. Fluid inclusion data have been previously collected to constrain the late exhumation history of the Himalayan units close to their main tectonic contacts. In particular, a fluid evolution characterised by influx of mixed CO_2-H_2O at amphibolite-facies conditions and of H_2O-NaCl fluids during greenschist-facies retrogression has been reported in rocks and veins across the Main Central Thrust in central Himalaya (Leroy *et al.*, 1975; Pêcher, 1978; Sauniac & Touret, 1983; Craw, 1990; Boullier *et al.*, 1991; Morrison & Oliver, 1993; Sachan *et al.*, 2001; Carosi *et al.*, 2005). A low-salinity aqueous fluid trapped at greenschist-facies conditions was also reported in quartz veins cross-cutting blueschist rocks from the Shergol Ophiolitic Melange of the W Himalaya (Sachan & Mukherjee, 2001).

Other fluid inclusion data have been collected on segregations and veins from the western Nanga Parbat syntaxis (*e.g.* Poage *et al.*, 2000) and the eastern Namche Barwa syntaxis (Craw *et al.*, 2005), in order to relate the fluid influx during their rapid uplift with surface springs originated from the thermal anomaly. These data indicate that, during uplift, the late CO_2-rich metamorphic fluids were diluted at shallow levels by influx of surface water. Significant differences on the nature and evolution of late fluids have been observed between Nanga Parbat and Namche Barwa (Craw *et al.*, 2005). Convincing evidence for fluid immiscibility in the upper 6 km of the crust, including boiling water at shallow levels (>3 km), has been reported in both syntaxes (Craw *et al.*, 1994; 1997; 2005; Winslow *et al.*, 1994).

Investigations on fluid inclusions trapped during subduction of continental crust and Himalayan metamorphism under high pressure (HP) conditions are still few. In fact, the only data available are from eclogites of the Tso-Morari Dome (NW Himalaya), where the fluid at 530–580 °C and 1.1–1.4 GPa is a moderate-salinity (11–13 wt % $NaCl_{eq}$) aqueous fluid (Sachan *et al.*, 1999).

A recent paper (Groppo *et al.*, 2007) describes in detail the metamorphic evolution of the only eclogites found so far in the eastern Himalaya (Ama Drime range, the Kharta region of Southern Tibet). In contrast to the Tso-Morari eclogites, those from the Ama Drime range did not experience ultra-high pressure (UHP) metamorphism and are characterised by a strong granulite-facies overprint.

Eclogites are very few in the Himalayas, and those of the Ama Drime range link rapid uplift from great depths to a

DOI: 10.1127/0935-1221/2007/0019-1748
0935-1221/07/0019-1748 $ 10.35

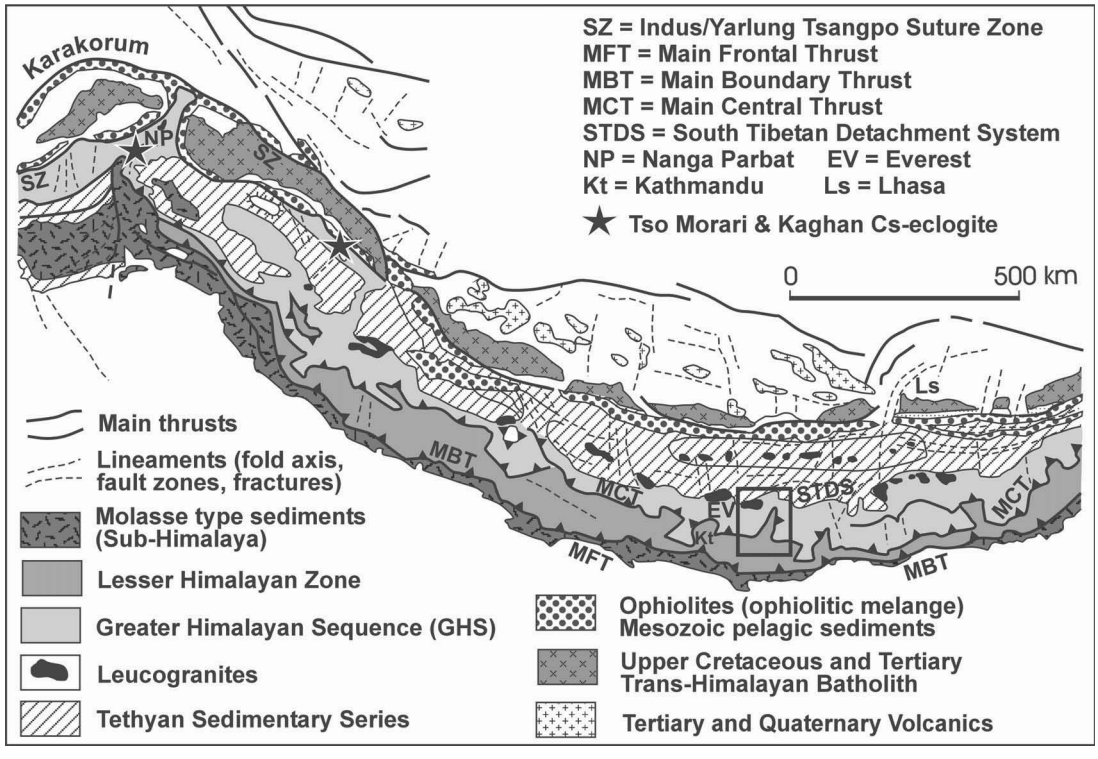

Fig. 1. Geological sketch map of the Himalaya and southern Tibetan Plateau (modified after Dietrich & Gansser, 1981). The Ama Drime range and Kharta region are shown in the box.

well constrained P-T path and good preservation of metamorphic fluids, making therefore highly advisable to study their fluid evolution.

In this paper we report the results of a fluid inclusion study on these granulitised eclogites and on an associated vein. The evolution of the fluid phase is discussed in relation to the P-T path and some speculation on the origin of the trapped fluids is also proposed. Three samples have been chosen for study because they are scarcely involved in the late stages of metamorphic evolution and preserve relics of eclogitic and granulitic fluids. To our knowledge, this is the first report on the nature and evolution of the fluid phase in Himalayan rocks from their HP metamorphic peak to the end of their exhumation path.

Geological setting

The Himalayan orogen is comprised of a number of E-W-trending lithotectonic units, separated by large-scale thrust systems dipping to the north (Fig. 1). From south to north, these units in Nepal are: the molasse sediments of the Sub-Himalaya, the Lesser Himalayan Zone, the Greater Himalayan Sequence (GHS), and the Tethyan Sedimentary Series (Upreti, 1999). The non-metamorphic to amphibolite-facies Lesser Himalayan Zone is separated from the molasse sediments by the Main Boundary Thrust (MBT) and from the high-grade metamorphic rocks of the GHS by the Main Central Thrust (MCT). The GHS is separated from the anchimetamorphic sedimentary rocks of the structurally higher Tethyan Sedimentary Sequence by the South Tibetan Detachment System (STDS; Fig. 1).

The studied samples occur at the northern end of the Arun Tectonic Window (ATW) in the Ama Drime range, a N-S trending ridge, 60 km long, lying to the east of the Phung Chu (upper Arun River) (Fig. 2). The ATW is the core of an arch-like structure of regional extent ("Trans-anticlinal de l'Arun"; Bordet, 1961) deflecting to the north the E–W trend of the north-dipping lithotectonic contacts, and extending from the lower Arun valley in east Nepal to the northern end of the Ama Drime range in southern Tibet (Fig. 2). From south to north the ATW shows a complete section of the Himalayan tectonic units, from the Lesser Himalayan Tumlingtar Unit (a thick sequence of Precambrian phyllites and quartzites with subordinated amounts of carbonatic phyllites and dolomite marbles; Meier & Hiltner, 1993) at the bottom, to the granulite-facies GHS of the upper Phung Chu and the Tethyan Sedimentary Series at the top (Fig. 2).

North of Tumlingtar and structurally upward, the low-grade Lesser Himalayan metasediments of the Tumlingtar Unit are separated by thrust sheets and ductile shear zones (the Main Central Thrust I according to the nomenclature of Arita, 1983) from the Khandbari and Num orthogneisses (Brunel, 1983; Lombardo *et al.*, 1993) and from metapelitic rocks showing a distinctly higher metamorphic grade (amphibolite-facies) relative to the Tumlingtar Unit (Milke Gneiss; Andrews, 1985). The amphibolite-facies orthogneisses and metapelites are hereby called Lesser Himalayan Crystalline Sequence

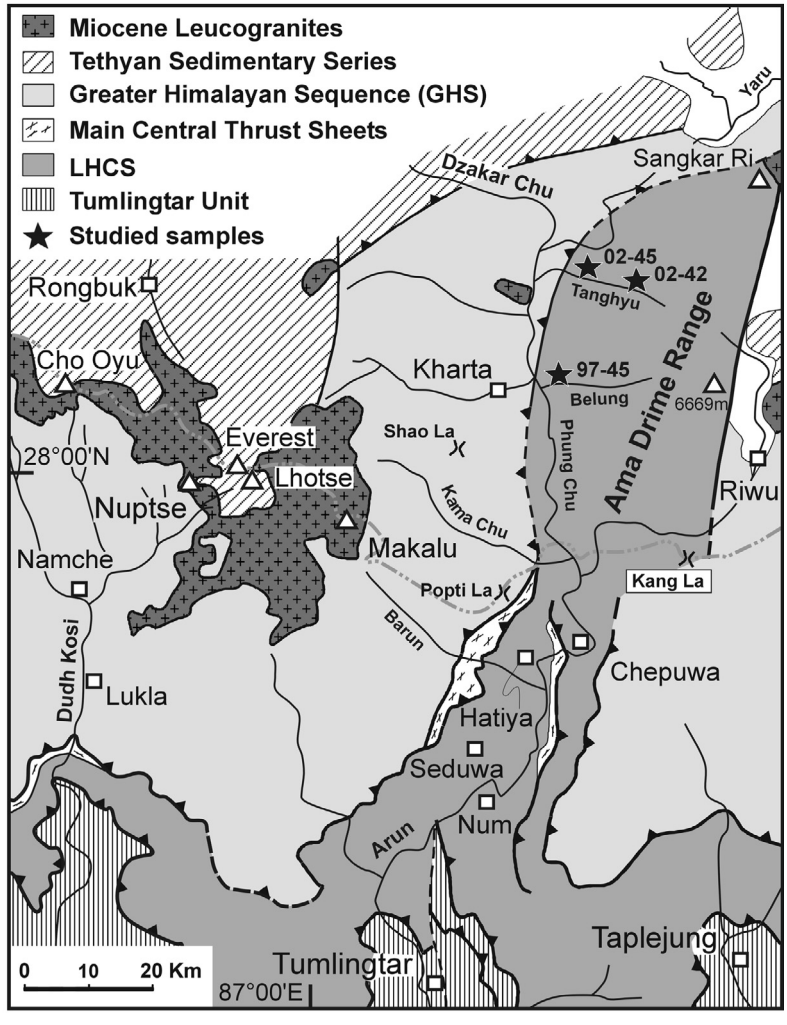

Fig. 2. Geological sketch map of the Kharta region and upper to middle Arun (Phung Chu) drainage, modified after Groppo *et al.* (2007). The map was compiled from the maps of Yin & Kuo (1978), Brunel (1983), Burg (1983), Lombardo *et al.* (1993), Bureau of Geology and Mineral Resources of Xizang Autonomous Region (1993), Carosi *et al.* (1998), Zhang & Guo (2007). Thick barbed lines are the Main Central Thrust I and II, thin barbed line is the South Tibetan Detachment System, solid lines are faults. Grey dashed line is the approximate political boundary between Nepal (to the south) and China (to the north).

(LHCS, Fig. 2), as is done in western–central Nepal for similar sequences (Upreti, 1999) and further west in the Sutlej Valley of Himachal Pradesh, India (Vannay *et al.*, 2004 and references therein). As is well displayed in the Num-Makalu section, metasedimentary and metagranitic thrust sheets with amphibolites (the Main Central Thrust II according to the nomenclature of Arita, 1983) separate the Num Orthogneiss of the LHCS from the overlying Barun Gneiss, the structurally lower unit of the GHS (Bordet, 1961; Brunel, 1983; Lombardo *et al.*, 1993; Goscombe & Hand, 2000).

North of the Nepal-China border, lithologies very similar to the Barun Gneiss are well exposed west of the Phung Chu in the Kharta region (Kharta Gneiss Complex of Borghi *et al.*, 2003). The Kharta Gneiss Complex consists of migmatitic garnet-bearing metapelites, with minor metabasites and calc-silicate rocks, equilibrated in granulite- to upper amphibolite-facies that host bodies of migmatitic, sillimanite- and cordierite-bearing orthogneiss. Migmatites are especially well developed in the lower Kharta valley and along the W side of the Phung Chu valley, where several generations of leucosomes are conspicuous and range in morphology from concordant leucogranitic orthogneiss containing garnet and prismatic sillimanite after kyanite, to discordant cordierite-bearing leucogranite veins and pods. Both the concordant leucogranitic orthogneiss and the discordant leucogranite veins are crosscut by Miocene leucogranite dykes (Visonà & Lombardo, 2002). Westward, in the upper Rongbuk valley, and northward, in the Dzakar Chu gorge, the GHS is bounded at the top by the extensional ductile to brittle shear zones of the STDS (Burg *et al.*, 1984; Burchfiel *et al.*, 1992; Carosi *et al.*, 1998; Cottle *et al.*, 2006).

Networks of dykes, sheet-like bodies and large laccolithic plutons of leucogranite occur in the GHS of the Phung Chu, upper Kama and Kharta Valleys, as well as in the North

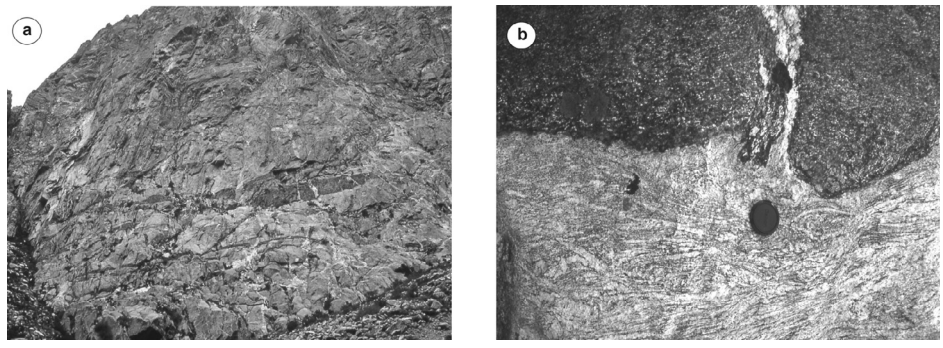

Fig. 3. (a) Eclogite boudins within granitic gneiss. View looking north. Field of view about 40 m. Tanghyu Valley, Kharta Region. (b) Detail of an eclogite boudin within migmatitic orthogneiss. Tanghyu Valley, Kharta Region.

Col Formation, the lowest portion of the Tethyan Sedimentary Series (Visonà & Lombardo, 2002). The granite plutons reach a thickness of 1–2 km in the Makalu massif and are composed of two-mica granite intruded by tourmaline granite. The generation and cooling of leucogranites in the Everest–Makalu region fall in the Early-Middle Miocene, between 24 and 16 Ma (Ferrara *et al.*, 1983; Schärer, 1984; Schärer *et al.*, 1986; Hodges *et al.*, 1998; Murphy & Harrison, 1999; Simpson *et al.*, 2000). Younger U-Th-Pb ages (12.4–12.8 Ma) were measured by Liu *et al.*(2007) on monazites from the granite body at Tongmen in the lower Dzakar Chu valley, close to the STD separating the GHS from the overlying North Col Formation.

East of the Phung Chu, i.e. in the western side of the Ama Drime range the high-grade rocks of the Kharta Gneiss Complex are separated from the underlying granitic orthogneisses by a north-trending belt of thrust sheets of granitic orthogneiss with garnet amphibolite, quartzite and mylonitic marble (Lombardo *et al.*, 1998; Lombardo & Rolfo, 2000). This geological setting is similar to the tectonic sequence observed north of Seduwa in the core of the ATW (Bordet, 1961; Lombardo *et al.*, 1993), where metasedimentary and metagranitic thrust sheets with amphibolites separate the granitic Num Orthogneiss belonging to the LHCS from the overlying Barun Gneiss, the basal unit of the GHS that is lithologically identical with the Kharta Gneiss Complex. This suggests that the Ama Drime orthogneiss may be homologous to the Num Orthogneiss and as such may belong to the LHCS rather than to the GHS. Irrespective of its interpretation as a thrust (Liu *et al.*, 2007; Groppo *et al.*, 2007) or as detachment (as argued by Cottle *et al.*, 2006) the shear zone bounding the Ama Drime orthogneiss to the west is a major lithotectonic break, as indicated by the difference in ε_{Nd} and Sm/Nd model ages of Tertiary leucogranites and country rocks (Visonà *et al.,* 2000; Liu *et al*., 2007). Model ages average 2.0 Ga in the GHS leucogranites and 2.9 Ga in the leucogranites hosted in the thrust sheets and further downsection in the granitic orthogneiss of the Ama Drime range. Such model ages are consistent with those determined by Robinson *et al.* (2001) on paragneisses from the base of the GHS and from granitic orthogneisses of the Lesser Himalayan Zone in eastern Nepal, which average 2.0 and 2.5 Ga, respectively. ε_{Nd} values are likewise distinctly lower in sillimanite gneiss of the Ama Drime relative to garnet-sillimanite gneiss and granite of the GHS (Liu *et al*., 2007).

The granulitised eclogites occur as both boudinaged dykes and small bodies of basaltic composition within the granitic orthogneisses. They were found during the 1997 field season in outcrops southeast of Kharta, along the eastern side of the Phung Chu valley (Lombardo et al., 1998). In the 1999 and 2002 field seasons, eclogites were found also in the east–west-trending valleys leading from the Phung Chu towards the interior of the Ama Drime range, in particular, in the Belung and Tanghyu Valleys (Fig. 2). Granulitised eclogites identical to those of the W side were described by Liu *et al.* (2005) on the eastern side of the Ama Drime range from N of Dinggye to W of Riwu.

In the studied outcrops, the granulitised eclogites are hosted within granitic orthogneisses, locally migmatitic, mainly consisting of K-feldspar, plagioclase, quartz and biotite (Fig. 3), with layers and intercalations of garnet-sillimanite-biotite gneisses and restitic garnet-biotite-sillimanite-gedrite-cordierite schists. Cottle *et al.* (2006) report $^{208}Pb/^{232}Th$ ages of 12.7 ± 0.8 Ma for monazite from leucosome and melanosome of a host migmatitic gneiss, for which zircon gave intercepts at 11.0 ± 3.3 and 1799±12 Ma. Monazite from an amphibolite-facies rock of the LHCS was dated with the U-Th-Pb method by Liu *et al.* (2007). A linear regression through all fractions yielded a lower intercept age of 13.4 ± 1 Ma.

Locally, the main foliation of the eclogites is transected by mm- to cm-thick undeformed metamorphic veins (Fig. 4a) and by leucogranite dykes. $^{208}Pb/^{232}Th$ ages of monazite in such a cross-cutting leucogranite dyke average 11.6 ± 0.4 Ma (Cottle *et al.*, 2006). A leucogranite dyke close to eclogite pods has given monazite U-Th-Pb ages around 13 Ma (Liu *et al.* , 2007, their sample 1303), interpreted as crystallisation ages.

Attempts at estimating the age of the eclogite metamorphism in the granulitised eclogites has so far given elusive results. Rolfo *et al*. (2005) dated zircon in eclogite EV02-45 from Tanghyu Valley by the U-Pb SHRIMP method. Ages ranging from 88 to 110 Ma, prevailing in the zircon cores, have been interpreted to represent a Cretaceous protolith age. The analysed zircon also shows very thin rims with low Th/U ratios (0.02–0.03), yielding young

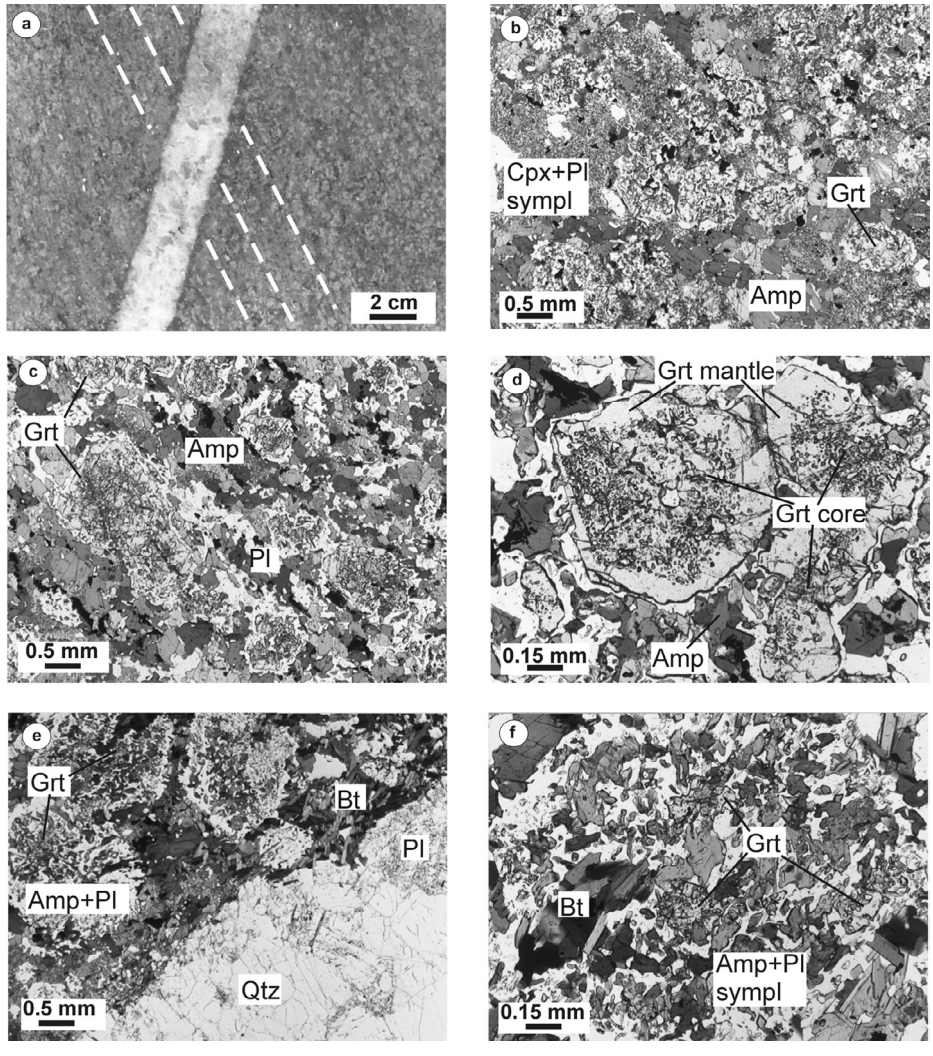

Fig. 4. Photographs showing the microstructure of the granulitised eclogites from the Kharta region. (a) Photograph of the Bt-Ap-Pl-Qtz vein cross-cutting the main foliation of the granulitised eclogite. The thick dashed lines point out the foliation. Sample EV02-45. (b) Microphotograph of undeformed sample where the pristine omphacite is totally replaced by a Cpx + Pl symplectite, while garnet is surrounded by moats of Pl + Opx. Sample EV02-42a; Plane Polarised Light (PPL). (c) Microphotograph sample EV97-45c where the orientation of amphibole and plagioclase defines a poorly foliation. PPL. (d) Microphotograph of porphyroblastic garnet with abundant inclusions of quartz and rutile in the core and an inclusion-free mantle. Sample EV97-45c, PPL. (e) Microphotograph showing strong retrogression of the granulitised eclogite near the coarse-grained vein. Note that the contact is marked by brown newly grown biotite and that garnet is replaced by an Amp + Pl + Bt aggregate. Sample EV02-45; PPL. (f) Detail of the Amp + Pl + Bt aggregate of Fig. 4e. Note the presence of a small relict of garnet. Sample EV02-45; PPL.

$^{206}Pb/^{238}U$ ages (12–15 Ma) interpreted as dating the end of the metamorphic fluid circulation and thus be linked to extrusion of the LHCS. Alternatively, as suggested by Groppo *et al.* (2007), growth of these zircon rims could result from breakdown of garnet to orthopyroxene + plagioclase and thus date a second granulitic event predating hydration of the granulitised eclogites. Young $^{206}Pb/^{238}U$ ages (17.6 ± 0.3 Ma) were also found by Li *et al.* (2003) with the SHRIMP U-Pb method on zircon rims from a high-pressure mafic granulite (actually a granulitised eclogite) of the northern Ama Drime range. Three zircon fractions from an eclogite of the western Ama Drime range, analysed by Liu *et al.* (2007), define a discordia line, with a lower intercept age of 10 ± 11 Ma and upper intercept age of 971 ± 8 Ma, interpreted as a crystallisation age, dating Neoproterozoic basic magmatic activity.

U-Pb zircon geochronology by Cottle *et al.* (2006) on an eclogite from the western side of the Ama Drime range yielded for 12 spot analyses of zircon rims intercepts at 0 ± 0 and 957 ± 18 Ma, suggesting a single phase of zircon growth at 960 Ma interpreted as protolith age.

Analytical methods

Chemical compositions of minerals were obtained with a *Cambridge Instruments* SEM Stereoscan 360 equipped with an EDS Energy 200 and a Pentafet detector (Oxford

Table 1. Representative minerochemical analysis of rock-forming minerals from granulitised eclogites EV97-45 (from Lombardo & Rolfo, 2000) and EV02-42 (from Groppo *et al.*, 2007).

Sample	**EV02-42**	**EV97-45**	**EV02-42**	**EV02-42**	**EV02-42**	**EV97-45**	**EV02-42**	**EV02-42**	**EV02-42**	**EV02-42**	**EV02-42**	**EV02-42**	**EV02-42**	**EV02-42**	**EV02-42**	**EV02-42**
Analysis	**7.10**	**S11.1**	**7.9**	**10.7**	**6.3**	**S1-2**	**6.8**	**9.8**	**14.3**	**1.4**	**6.9**	**15.5**	**15.6**	**7.23**	**7.3**	**14.29**
Mineral	**Grt core**	**Grt core**	**Grt mantle**	**Cpx in Grt**	**Cpx in sympl**	**Cpx in sympl**	**Opx in sympl**	**Amp after Omp**	**Amp in corona**	**Matrix Amp**	**Pl in sympl Omp**	**Pl in sympl Phe**	**Pl in sympl Phe**	**Pl in Grt**	**Pl in corona**	**Matrix Pl**
SiO2	37.68	38.12	37.34	51.30	50.27	51.82	50.62	42.35	42.39	42.55	56.81	54.58	63.07	51.32	55.45	60.98
TiO2	0.00	0.00	0.00	0.00	0.00	0.00	0.00	1.90	1.57	1.28	0.00	0.00	0.00	0.00	0.00	0.00
Al2O3	21.00	20.58	20.79	7.70	2.09	3.28	0.77	10.87	11.27	11.58	27.17	28.54	23.01	29.56	27.22	23.91
Fe2O3	2.81	1.60	3.00	1.97	4.83	0.00	1.73	3.26	3.42	4.07	0.00	0.00	0.00	0.00	0.00	0.00
FeO	23.15	24.24	24.60	7.19	6.99	9.43	29.97	17.09	15.12	12.82	0.66	0.00	0.00	1.75	0.73	0.00
MnO	0.00	0.00	0.82	0.00	0.00	0.00	0.57	0.00	0.00	0.00	0.00	0.00	0.00	0.00	0.00	0.00
MgO	3.44	4.09	2.97	9.47	11.88	12.38	16.41	8.38	9.42	10.43	0.00	0.00	0.00	0.00	0.00	0.00
CaO	12.31	10.97	10.86	19.57	23.48	21.69	0.57	11.92	12.38	11.97	9.92	12.04	5.18	13.59	10.92	6.09
Na2O	0.00	0.00	0.00	2.63	0.40	0.82	0.00	1.58	1.64	1.73	6.18	5.03	8.42	4.14	5.50	7.93
K2O	0.00	0.00	0.00	0.00	0.00	0.00	0.00	0.87	0.89	0.59	0.00	0.00	0.24	0.00	0.00	0.00
Total	100.39	99.60	100.38	99.83	99.94	99.42	100.64	98.22	98.10	97.02	100.74	100.19	99.92	100.36	99.82	98.91
Si	2.95	3.00	2.94	1.90	1.90	1.94	1.96	6.41	6.37	6.39	2.54	2.46	2.81	2.33	2.51	2.75
Al IV	0.00	0.00	0.00	0.10	0.00	0.00	0.04	1.59	1.63	1.61	0.00	0.00	0.00	0.00	0.00	0.00
Al VI	1.94	1.91	1.93	0.23	0.09	0.14	0.00	0.34	0.37	0.44	1.43	1.52	1.21	1.58	1.45	1.27
Ti	0.00	0.00	0.00	0.00	0.00	0.00	0.00	0.22	0.18	0.14	0.00	0.00	0.00	0.00	0.00	0.00
Fe3+	0.17	0.09	0.18	0.06	0.14	0.00	0.05	0.37	0.39	0.46	0.00	0.00	0.00	0.00	0.00	0.00
Fe2+	1.52	1.59	1.62	0.22	0.22	0.30	0.97	2.16	1.90	1.61	0.02	0.00	0.00	0.07	0.02	0.00
Mn	0.00	0.00	0.05	0.00	0.00	0.00	0.02	0.00	0.00	0.00	0.00	0.00	0.00	0.00	0.00	0.00
Mg	0.40	0.48	0.35	0.52	0.67	0.71	0.95	1.89	2.11	2.33	0.00	0.00	0.00	0.00	0.00	0.00
Ca	1.03	0.92	0.92	0.78	0.95	0.87	0.02	1.93	1.99	1.92	0.48	0.58	0.25	0.66	0.53	0.29
Na	0.00	0.00	0.00	0.19	0.03	0.06	0.00	0.46	0.48	0.51	0.54	0.44	0.73	0.36	0.48	0.69
K	0.00	0.00	0.00	0.00	0.00	0.00	0.00	0.17	0.17	0.11	0.00	0.00	0.01	0.00	0.00	0.00
Grs	0.27	0.26	0.22													
Alm	0.51	0.53	0.55													
Prp	0.14	0.16	0.12													
Sps	0.00	0.00	0.02													
Andr	0.08	0.05	0.09													
Ab											0.53	0.43	0.74	0.36	0.48	0.70
An											0.47	0.57	0.25	0.65	0.52	0.30
Or											0.00	0.00	0.01	0.00	0.00	0.00

Instruments) at the Department of Mineralogical and Petrological Sciences, University of Torino (Italy). Operating conditions were 15 kV accelerating voltage and 50 s counting time. SEM-EDS quantitative data (spot size = 2 μm) were acquired and processed using the Microanalysis Suite Issue 12, INCA Suite version 4.01; the raw data were calibrated on natural mineral standards and the $\Phi\rho$Z correction (Pouchou & Pichoir, 1988) was applied. Structural formulae of garnet, clinopyroxene, and plagioclase were processed using the software of Ulmer (1986). Amphiboles were classified according to the nomenclature of Leake *et al.* (2004). Mineral abbreviations are after Kretz (1983). In order to estimate the temperature conditions of vein forming, the hornblende-plagioclase geothermometer (Holland and Blundy, 1994; accuracy ±35 °C) was used.

Microthermometry of fluid inclusions within doubly polished, 100 μm thick sections was performed using a Linkam THMSG600 heating-freezing stage coupled with an Olympus polarizing microscope (100x objective) at the Department of Mineralogical and Petrological Sciences, University of Torino (Italy). The accuracy, estimated using synthetic fluid inclusion standards, is about 0.2 °C at the triple point of CO_2. Freezing temperature (*Tf*), triple point of CO_2 (Ttp_{CO2}), eutectic temperature of H_2O (Te_{H2O}), final melting temperature of hydrohalite, ice and clathrate (Tm_{Hhl}, Tm_{ice}, and Tm_{clat}), and homogenisation temperature of CO_2 in the liquid, or in the vapour or at critical conditions (ThL_{CO2}, ThV_{CO2}, ThC_{CO2}) were measured. Heating rates were always of 0.1 °C/min near *Te* and *Tm*, and 0.5 °C/min near *Th*. Fluid inclusion compositions, densities, and isochores were determined using the software packages CLATHRATES (Bakker, 1997) and FLUID (Bakker, 2003) in the version available in the CD-ROM that accompanies the paper by Bakker & Brown (2003).

Laser Raman analyses were made with a Labram microspectrometer (Jobin Yvon, Ltd) at the Department of Earth Sciences, University of Siena (Italy). A polarised Ar^+-ion laser operating at 514.5 nm wavelength and 200 mW incident power, was used as the excitation source. The laser spot size was focussed to 1–2 μm. Accumulation time was 20 seconds. Calibration was performed by using the 1332 cm^{-1} diamond band.

Petrography and mineral-chemistry

The granulitised eclogite

The three samples containing eclogite relics that were studied in detail are EV97-45, EV02-42, and EV02-45 (Fig. 2). Mineral chemistry (Table 1) and metamorphic evolution of sample EV97-45 was already reported by Lombardo & Rolfo (2000), while those of sample EV02-42 was recently studied by Groppo *et al.* (2007). A new sample (EV02-45, Table 2) was characterised in this study, because of its importance for constraining both the fluid and metamorphic evolution.

The granulitised eclogites are fine-grained and mainly consist of porphyroblastic garnet, clinopyroxene, plagioclase, brown amphibole and minor orthopyroxene, biotite, quartz and ilmenite. They can have equant structure (Fig. 4b) or show a preferred dimensional orientation of nematoblastic brown amphibole defining a poorly developed foliation (Fig. 4c).

On the basis of microstructural observations and mineral relationships, four mineral assemblages have been recognised: eclogite-facies assemblage M1; granulite-facies assemblage M2; coronitic assemblage M3; low-pressure – medium/high-temperature (LP – M/HT) assemblage M4.

The *eclogite-facies assemblage M1* consists of garnet, omphacite, minor quartz and phengite. Relics of eclogitic garnet, characterised by abundant inclusions of quartz and rutile, constitute the core of most porphyroblasts (Fig. 4d). Garnet cores are relatively Ca-rich with average composition $Alm_{49–55}Prp_{10–17}Grs_{19–31}Sps_{0–4}Adr_{1–14}$ (Fig. 5a). Unlike the relics of eclogitic garnet, both omphacite and phengite are totally replaced by symplectites of Cpx + Pl and of Bt + Pl, respectively (assemblage $M1_{dec}$). The clinopyroxene in the symplectite is a diopside, with less than 5 mol % of both jadeite and aegirine components (Fig. 5b). The plagioclase in the symplectite after omphacite is an andesine showing irregular zoning from An_{40} to An_{48}, whereas plagioclase in the symplectite after phengite is strongly zoned with an oligoclase core ($An_{21–25}$) and a labradorite rim ($An_{55–57}$; Fig. 5c).

The *granulite-facies assemblage M2* is represented by garnet rim and by relatively coarse-grained clinopyroxene, orthopyroxene and plagioclase, and by accessory ilmenite. The granulitic garnet rim is inclusion-free (Fig. 4d) and, relative to M1 garnet,, its composition is characterised by an increase of Fe and a decrease of Ca ($Alm_{51–58}Prp_{10–14}Grs_{14–25}Sps_{1–4}Adr_{7–15}$; Fig. 5a). The clinopyroxene has the same composition of that in the symplectites after omphacite. In the orthopyroxene, the $X_{Fe}(Opx)$ [$X_{Fe}(Opx) = Fe^{2+}/(Fe^{2+}+Mg)$] ranges from 0.51 to 0.59 and the Ca-content is less than 5 mol%. The plagioclase is a labradorite with anorthite component from An_{50} to An_{57} (Fig. 5c).

The *coronitic assemblage M3* is represented by a plagioclase + orthopyroxene ± amphibole corona developed around the garnet porphyroblasts. The inner part of the corona consists of radiating laths of plagioclase with composition ranging between An_{50} and An_{57} (Fig. 5c). The outer part of the corona consists of orthopyroxene compositionally similar to that of M2 assemblage, minor ilmenite, and amphibole with pargasitic to Fe-pargasitic composition.

The *LP – M/HT assemblage M4*, consisting of brown amphibole and plagioclase, is well developed in the rock matrix, where the brown amphibole locally defines the foliation. This assemblage may also replace former minerals in the symplectite after omphacite and in the corona around garnet. The amphibole is a pargasite and it is slightly zoned, with Na and Al^{VI} contents decreasing from core to rim (Fig. 5d). In sample EV02-45 the composition of matrix amphibole ranges from ferropargasite to hastingsite with Al^{IV} = 1.66–1.81 and Al^{VI} = 0.35–0.46 (Fig. 5d). The plagioclase composition varies from oligoclase to andesine ($An_{29–35}$; Fig. 5c).

The vein

In eclogite EV02-45, the main foliation is crosscut by a white vein about 2 cm thick (Figs. 4a and 4e). The vein consists of coarse-grained quartz, plagioclase, apatite and minor brown biotite. Plagioclase composition varies from oligoclase to andesine (An_{25-33}; Fig. 5c).

Close to the vein, the host rock is strongly retrogressed with development of a *vein-related assemblage M5* (Fig. 4e) consisting of brown biotite and green amphibole rimming the M4 brown amphibole. Besides, garnet porphyroblasts are almost totally replaced by an aggregate of green amphibole + plagioclase + brown biotite (Fig. 4f). The amphibole is hastingsitic or ferrotschermakitic in composition with $Al^{IV} = 1.57–1.68$ and $Al^{VI} = 0.27–0.39$ (Fig. 5d). The plagioclase is andesine showing a Ca-rich core (An_{38-50}) and a Ca-poor rim (An_{35-37}; Fig. 5c).

Fluid inclusion study

Fluid inclusion occurrence

The occurrence of a vein crosscutting the main foliation of the eclogite was extremely useful to define the different "groups of synchronous inclusions" (GSI, Touret, 2001) and their relative chronology. Six distinct GSI were recognised in the studied samples and are schematically described in Fig. 6 and Table 3. In particular, a careful fluid inclusion petrography made possible to distinguish the inclusions present only in the rock-forming minerals of the granulitised eclogite, i.e. the inclusions trapped during the early metamorphic stages, from the inclusions hosted in both vein and eclogite, i.e. the inclusions trapped during the late metamorphic stages. The first group is represented by aqueous or gaseous inclusions occurring in garnet, amphibole, and quartz; the second group consists of mixed CO_2-H_2O or aqueous inclusions found in quartz from the eclogite and in quartz and apatite from the vein.

Type I: saline aqueous-carbonate inclusions

The first type (Type I) consists of very rare and isolated (i.e. primary; Roedder, 1984) inclusions occurring only in the eclogitic core of the garnet (Fig. 6 and 7a; Table 3). The size of the inclusions is small, ranging from 5 to 10 μm in diameter, and evidence for partial decrepitation is common. Type I are three-phase (S+L+V) aqueous inclusions, all of them containing a colourless solid with high birefringence (Mg-calcite at the microRaman spectroscopy) that constitutes less than 30 % of the total volume of the inclusion.

Type II: carbonic-carbonate inclusions

Type II inclusions occur as isolated inclusions or as intragranular trails "grain internal" (see van der Kerkhof & Hein, 2001) within the granulitic mantle of garnet (Fig. 6 and 7b; Table 3). They have irregular shape and very small size (<7 μm), and commonly show evidence for partial decrepitation. Both two-phase (S + L) or three-phase (S+L+V) gaseous inclusions are observed at room temperature. All inclusions contain a colourless solid with high birefringence (Mg-calcite at the microRaman spectroscopy) that may constitute up to 40 % of the total volume of the inclusion.

Type III: aqueous inclusions with minor CO_2

Type III inclusions occur as very rare isolated inclusions within the brown pargasitic amphibole from assemblage M4 (Fig. 6 and 7c; Table 3). Besides, they are abundant in matrix quartz of the eclogite, where they occur as isolated inclusions and, rarely, as intragranular trails "from a grain boundary to another" (see van der Kerkhof & Hein, 2001). They are very small, their size ranging from less than 3 up to 10 μm in diameter, and are characterised by irregular shape. The inclusions are two-phase (L+V) aqueous inclusions with degree of filling (df = L/L+V) of 75–80.

Type IV: aqueous-carbonic inclusions

Type IV is the first GSI observed both in the vein and in the hosting eclogite (Fig. 6; Table 3). In the vein, it occurs as primary inclusions in quartz and apatite (Fig. 6 and 7d), whereas in matrix quartz of the eclogite it usually occurs as intragranular trails "grain internal" (Fig. 7e) or as rare isolated inclusions (Fig. 6). They are easily identifiable from other fluid inclusion types by their bigger size - varying from 10 to 20 μm in diameter - and by their negative crystal shape. All inclusions are three-phase aqueo-carbonic (V_{CO2}-L_{CO2}-L_{H2O}) and CO_2 represents 55–60 % of the inclusion total volume.

Type V: carbonic inclusions with minor H_2O

Type V inclusions are not abundant. They occur as intragranular trails only in quartz from both vein and eclogite (Fig. 6; Table 3). Rare intragranular trails "from a grain boundary to another" crosscut intragranular trails "grain internal" consisting of Type IV fluid inclusions (Fig. 7e). They have a very small size (<7 μm in diameter) and usually show an irregular shape. The inclusions appear to be two-phase gaseous inclusions, i.e. V_{CO2} and L_{CO2}. Nevertheless, some inclusions clearly show the presence of water at the corners (Fig. 7e), suggesting that probably all the inclusions contain water up to 30 % of the inclusion total volume. The different occurrence of Type IV and Type V fluid inclusions, their different size and shape, and the absence of synchronous inclusions lacking CO_2 or H_2O allow us to exclude that Type IV and Type V fluid inclusions may represent a single heterogeneous trapping of two immiscible liquids.

Table 2. Representative minerochemical analyses of rock-forming minerals from granulitised eclogite and vein (sample EV02-45).

Sample	EV02-45	EV02-45	EV02-45	EV02-45	EV02-45	EV02-45	EV02-45	EV02-45	EV02-45	EV02-45	EV02-45	EV02-45	EV02-45	EV02-45	EV02-45
Analysis	1Grt37	5Grt14	1Grt35	1Grt38	S1Cpx1s	4Amp3	1Amp65	1Amp69	4Amp7	1Amp67	1Amp68	4Pl5	4Pl9	1Pl40	2Pl56
Mineral	Grt core	Grt core	Grt mantle	Grt mantle	Cpx in sympl	Matrix Amp	Matrix Amp	Matrix Amp	Amp after Grt	Amp after Grt	Amp after Grt	Pl core after Grt	Pl rim after Grt	Pl in vein	Pl in vein
SiO2	37.23	37.03	36.94	36.88	50.20	39.93	40.22	40.46	41.26	40.38	41.69	56.58	59.72	60.82	62.85
TiO2	0.00	0.00	0.00	0.00	0.00	0.99	1.33	1.63	0.87	1.26	1.11				
Al2O3	20.36	20.50	20.15	20.50	1.39	12.08	11.96	11.49	10.85	10.99	10.12	27.03	24.63	24.71	23.16
Fe2O3	3.55	3.33	3.68	3.56	5.41	5.76	5.46	3.17	4.53	6.00	6.97				
FeO	22.91	24.48	22.85	23.32	8.66	19.14	14.96	17.45	19.48	15.00	14.21				
MnO	0.50	1.55	0.63	1.13	0.00	0.56	0.00	0.00	0.00	0.00	0.51				
MgO	2.60	2.86	2.54	2.81	11.41	5.20	7.67	7.11	6.09	7.32	7.51				
CaO	12.85	10.25	12.61	11.42	22.67	12.00	12.06	11.55	11.84	11.96	12.17	10.45	7.08	6.72	5.21
Na2O	0.00	0.00	0.00	0.00	0.43	1.39	1.46	1.34	1.38	1.35	1.16	5.73	7.35	7.65	8.43
K2O	0.00	0.00	0.00	0.00	0.00	1.10	0.93	1.04	0.98	0.89	1.04	0.00	0.00	0.00	0.00
Total	100.01	100.00	99.40	99.62	100.18	98.15	96.05	95.24	97.28	95.15	96.49	99.80	99.23	99.90	99.65
Si	2.95	2.94	2.94	2.93	1.91	6.19	6.23	6.34	6.41	6.32	6.43	2.55	2.69	2.72	2.80
Al IV						1.81	1.77	1.66	1.59	1.68	1.57				
Al VI	1.90	1.92	1.89	1.92	0.06	0.40	0.41	0.46	0.39	0.35	0.27	1.44	1.31	1.30	1.22
Ti	0.00	0.00	0.00	0.00	0.00	2.21	2.18	2.12	1.99	2.03	1.84				
Fe3+	0.21	0.20	0.22	0.21	0.15	0.67	0.64	0.37	0.53	0.71	0.81				
Fe2+	1.52	1.63	1.52	1.55	0.28	2.48	1.94	2.29	2.53	1.96	1.83				
Mn	0.03	0.10	0.04	0.08	0.00	0.07	0.00	0.00	0.00	0.00	0.07				
Mg	0.31	0.34	0.30	0.33	0.65	1.20	1.77	1.66	1.41	1.71	1.73				
Ca	1.09	0.87	1.08	0.97	0.92	1.99	2.00	1.94	1.97	2.00	2.01	0.51	0.34	0.32	0.25
Na	0.00	0.00	0.00	0.00	0.03	0.42	0.44	0.41	0.42	0.41	0.35	0.50	0.64	0.66	0.73
K	0.00	0.00	0.00	0.00	0.00	0.22	0.18	0.21	0.19	0.18	0.20	0.00	0.00	0.00	0.00
Grs	0.26	0.20	0.25	0.22											
Alm	0.52	0.55	0.52	0.53											
Prp	0.10	0.12	0.10	0.11											
Sps	0.01	0.04	0.01	0.03											
Andr	0.11	0.10	0.11	0.11											
Ab												0.50	0.65	0.67	0.75
An												0.50	0.35	0.33	0.26
Or												0.00	0.00	0.00	0.00

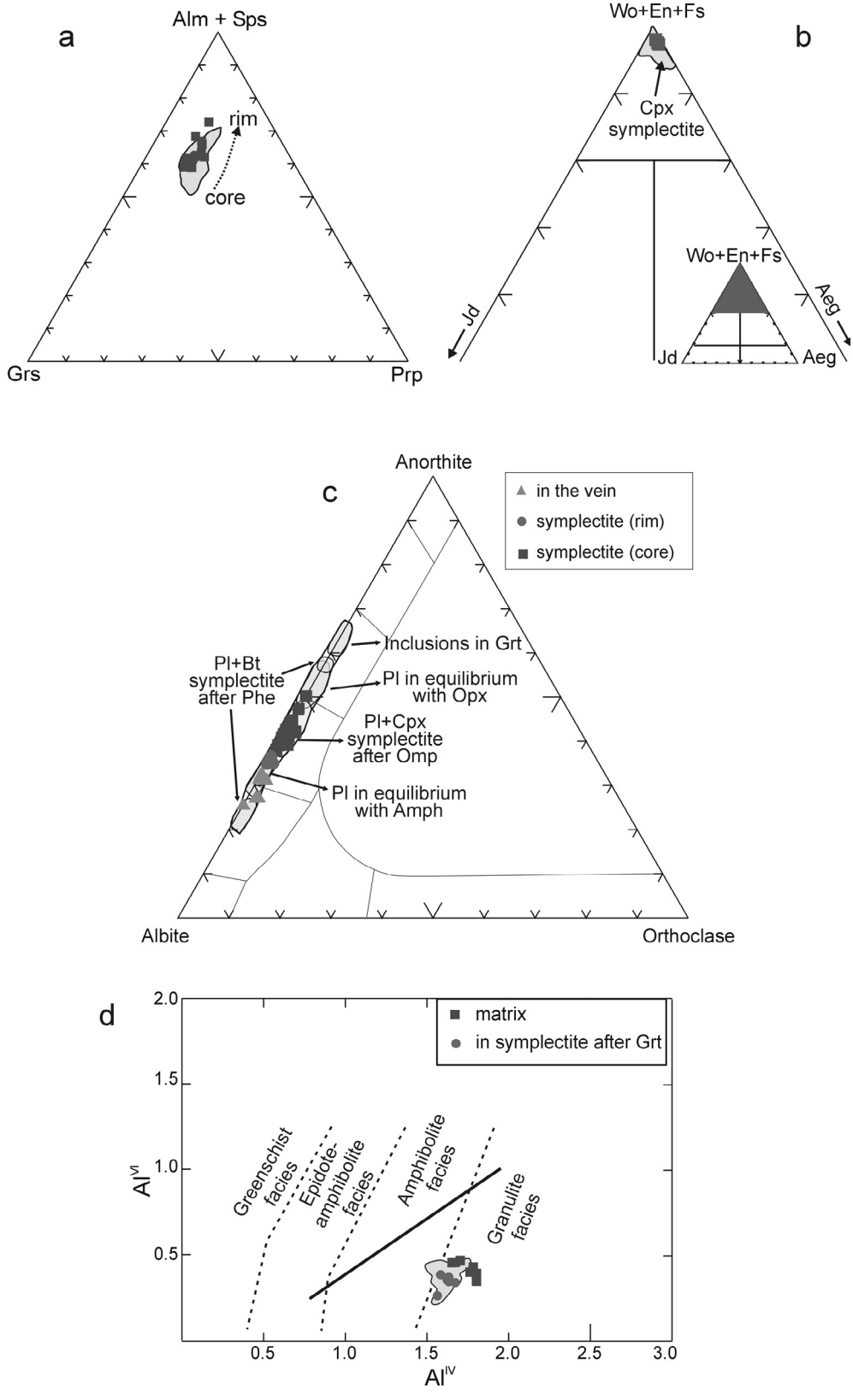

Fig. 5. Chemical compositions of garnet, clinopyroxene, plagioclase, and amphibole respectively plotted (a) in the (almandine+spessartine)-grossular-pyrope diagram, (b) in the (wollastonite+enstatite+ferrosilite)-jadeite-aegirine diagram of Morimoto (1988), (c) in the albite-anorthite-orthoclase diagram, and (d) in an Al^{VI} *versus* Al^{IV} diagram. The distinction between low-P and high-P amphiboles (solid line) is from Raase (1974) and that among amphibole composition in the different metamorphic facies is from Zakrutkin (1968). The light grey area in the diagrams corresponds to mineral compositions reported in Lombardo & Rolfo (2000) and in Groppo *et al.* (2007).

Table 3. Nature and occurence of the six different groups of synchronous inclusions (GSI) recognised in the studied samples of the Ama Drime eclogites.

GSI	nature of the fluid	occurrence in eclogite			occurrence in vein	
		Grt (M1-M2)	Amp (M4)	Qtz	Ap (M5)	Qtz
Type I	saline aqueous-carbonate	isolated in Grt core (M1)				
Type II	carbonic-carbonate	isolated or grain-internal trails in Grt mantle (M2)				
Type III	aqueous with minor CO_2		isolated	isolated		
Type IV	aqueous-carbonic			intragranular trails	isolated	isolated
Type V	carbonic with minor H_2O			intragranular trails		intragranular trails
Type VI	pure water			intragranular and transgranular trails		intragranular and transgranular trails

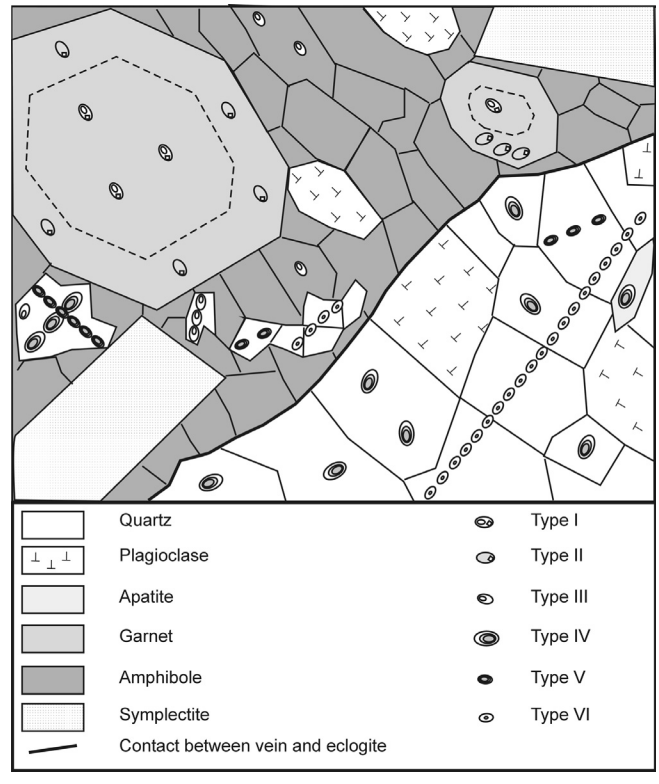

Fig. 6. Cartoon summarising the occurrence, in both eclogite and vein, of the six groups of synchronous inclusions recognised in the Ama Drime samples.

Type VI: pure water inclusions

Type VI fluid inclusions constitute intragranular and transgranular trails in quartz of both the vein and host eclogite (Fig. 6 and 7f). The inclusions, up to 10 μm in size, are elongated and show irregular shape. They are two-phase (L + V) aqueous inclusions with df = 80–90.

Microthermometry, fluid composition and density calculation

Representative microthermometric data of the six GSI are reported in Table 4.

Type I: saline aqueous-carbonate inclusions

Freezing temperature (Tf) of Type I inclusions ranges between –52.6 and –45.9 °C and eutectic temperature (Te_{H2O}) varies from –30.1 to –28.9 °C (Fig. 8a). Both data sets suggest the presence of Mg^{2+} and/or Fe^{2+}, in addition to Na^{+}, as dissolved cations in the fluid. Melting temperature of hydrohalite (Tm_{Hhl}) is between –24.1 and –21.7 °C (with majority at –22.1 °C), and melting temperature of ice (Tm_{ice}) varies between –7.2 and –6.5 °C (with majority at –6.5 °C), indicating medium salinity. The homogenisation is to the liquid (L+V –> L) and temperatures (ThL_{H2O}) range

from 145.3 to 218.7 °C, with an asymmetric distribution and a peak at about 218 °C (Fig. 8b).

All these data show that Type I fluid inclusions at present contain a high-density (0.99–0.92 g/cm^3) - medium-salinity aqueous fluid (4.5 NaCl and 5.5 $MgCl_2$eq wt%; Bakker, 2003). Nevertheless, the presence of Mg-calcite daughter minerals in the inclusions suggests that, during trapping, the fluid was not a pure aqueous fluid, but probably contained CO_2. Possibly, during metamorphic evolution the carbonate precipitated in consequence of a reaction of the brine with carbonic acid.

Type II: carbonic-carbonate inclusions

Type II fluid inclusions melt instantaneously (S+V → L+V) at temperatures very close to the triple point of pure CO_2 (-56.6 °C). The homogenisation is usually to the liquid and ThL_{CO2} ranges from 3.2 to 29.9 °C. Few critical homogenisations (L+V –> C) are observed at ThC_{CO2} = 30.9 – 31.0 °C. The resulting histogram is asymmetric with most measurements around 26.8 °C (Fig. 9a).

These microthermometric data indicate that Type II fluid inclusions are filled by pure CO_2 with density from 0.41 to 0.91 g/cm^3.

Type III: aqueous inclusions with minor CO_2

Type III fluid inclusions freeze at Tf between –50.0 and –40.0 °C and Te_{H2O} varies from –35.2 to –28.1 °C (Fig. 8c). These data are compatible with the presence in the fluid of divalent cations, such as Mg^{2+} and/or Fe^{2+}, in addition to Na^+. Tm_{Hhl} ranges from –21.8 to –18.1 °C (with majority at –20.4 °C), and Tm_{ice} is from –4.2 and –1.1 °C (with majority at –2.7 °C), i.e. lower than that of type I fluid inclusions (Fig. 10). In some inclusions, dissolution of clathrate is clearly observed at very constant temperature (Tm_{clath} = 8.2–8.4 °C). This indicates that minor amounts of CO_2 are dissolved in the fluid, and that the salinity is low, in agreement with the low Tm_{ice} measured. The homogenisation is always into the liquid and ThL_{H2O} varies from 153.8 to 234.5 °C, with a symmetric distribution and a peak at about 206 °C (Fig. 8d).

On the basis of these data, the fluid trapped in Type III fluid inclusions is a low-salinity - low-density (0.80 g/cm^3) aqueous fluid with minor amount of dissolved CO_2 (X_{H2O} = 0.95, X_{CO2} = 0.03, X_{NaCl} = 0.01, X_{MgCl2} = 0.01).

Type IV: aqueous-carbonic inclusions

Phase transitions in the aqueous part of Type IV inclusions are very difficult to observe, due to the high amount of CO_2. Where observable, Tf is from –49.0 to –28.0 °C, Te_{H2O} is near the eutectic temperature of NaCl- H_2O system (–20.8 °C), and Tm_{ice} is from –4.6 and –4.1 °C. On the contrary, the dissolution of clathrate is more recognisable and occurs at Tm_{clath} from 7.3 to 9.6 °C (with majority at 8.2 °C; Fig. 9d). The carbonic part of fluid inclusions melts instantaneously (S+V → L + V) at temperatures very close to –56.6 °C. The CO_2 homogenisation is always to the liquid and ThL_{CO2}, from 27.1 to 30.9 °C, make a symmetric histogram with peak at 29.1 °C (Fig. 9c). Total homogenisation temperature of fluid inclusions (L_{CO2} + L_{H2O} –> homogeneous fluid) could not be measured, since inclusions decrepitated during heating.

Microthermometric data indicate that the fluid trapped in Type IV inclusions is a low-density (0.77 g/cm^3) aqueo-carbonic fluid (X_{H2O} = 0.67, X_{CO2} = 0.31, X_{NaCl} = 0.02).

Type V: carbonic inclusions with minor H_2O

Microthermometric data of Type V fluid inclusions are measurable just from the biggest inclusions. The only phase transitions observable in the aqueous part is dissolution of clathrate at Tm_{clath} from 7.9 to 9.2 °C with three peaks at 8.3, 8.5, and 9.1 °C (Fig. 9b), suggesting the presence of small amounts of a low-salinity aqueous phase. The carbonic part of fluid inclusions melts instantaneously (S+V → L+V) at a temperature very close to the triple point of pure CO_2 (–56.6 °C). In most inclusions the carbonic part is only vapour, but some inclusions show homogenisation into the vapour (L + V –> V) at temperatures (ThV_{CO2}) between 22.2 and 22.6 °C. Total homogenisation temperature could not be measured, in order to prevent decrepitation of the inclusions.

These data indicate that the fluid has composition X_{H2O} = 0.54, X_{CO2} = 0.44, X_{NaCl} = 0.02 and density 0.82 g/cm^3.

Type VI: pure water inclusions

In spite of their abundance, only few Type VI inclusions are large enough to observe the phase transitions. The inclusions freeze at Tf between –42.0 and –34.0 °C (Fig. 8e), and Te_{H2O} ranges from –20.7 to –17.3 °C, i.e. close to the eutectic temperature of the NaCl- H_2O system. Final melting of ice occurs at high temperatures (Fig. 10), i.e. from –0.7 to –0.3 °C (with majority at –0.6 °C). The homogenisation is into the liquid and ThL_{H2O} are very scattered, ranging from 136.3 to 374.3 °C (Fig. 8f) with a poorly defined peak at 217.9 °C.

Microthermometric data indicate that the trapped fluid is an aqueous fluid characterised by very-low salinity (1.0 NaCl wt %) and low-density (from 0.94 to 0.51 g/cm^3).

Discussion

Petrological constraints on the metamorphic evolution of the granulitised eclogites and the associated vein

Four metamorphic stages have been previously recognised by Groppo *et al.* (2007) in the granulitised eclogite EV02-42 and host gneiss, on the basis of microstructural data and linking P-T pseudosections (Connolly, 1990) with conventional thermobarometry.

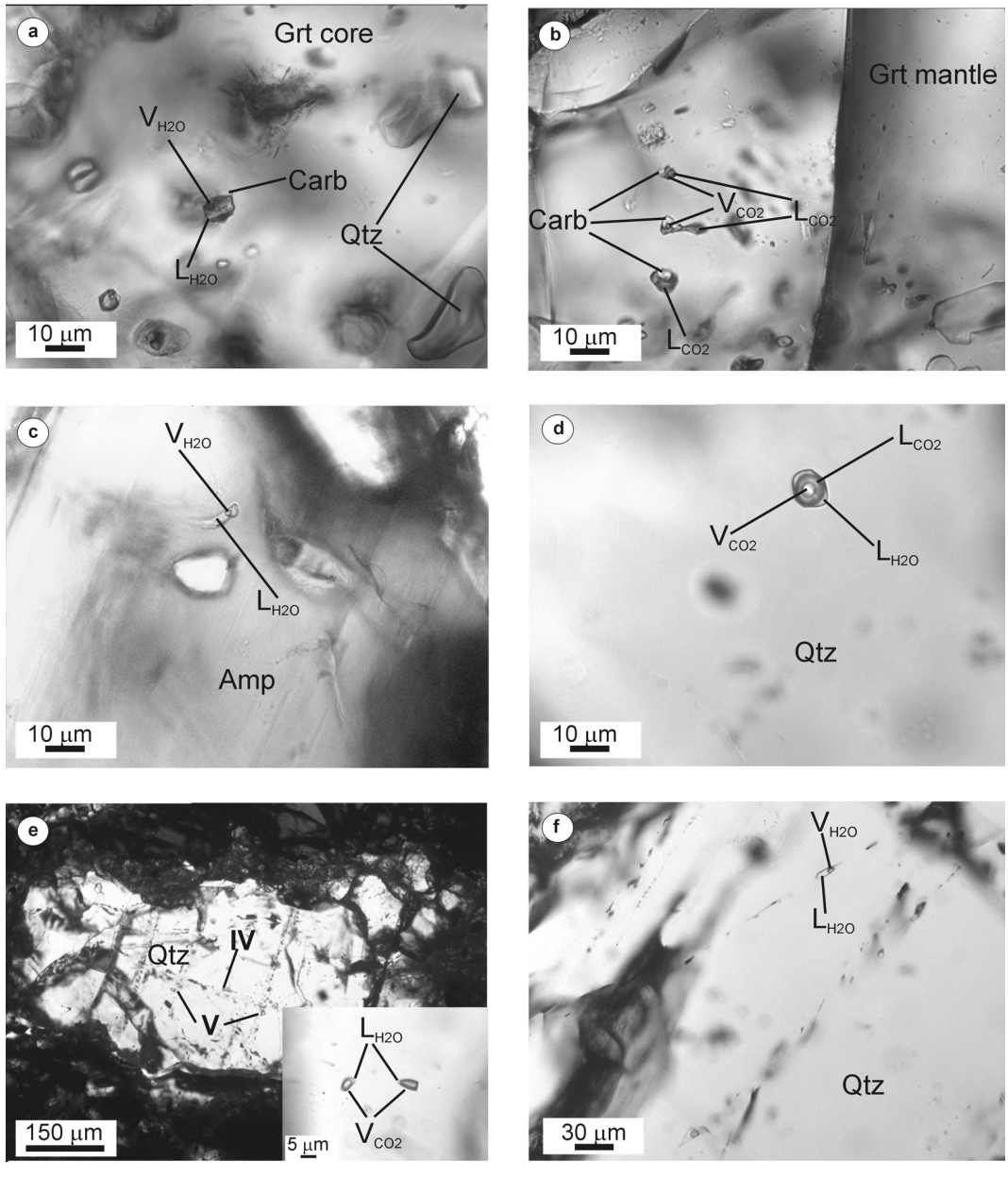

Fig. 7. Photomicrographs of fluid inclusions in the granulitised eclogites from Ama Drime range and associated vein. (a) Isolated Type I three-phase aqueous inclusions in the garnet core. Note the blebs of quartz, a typical mineral inclusion within the Grt core, and the presence of decrepitated fluid inclusions. Sample EV97-45b; PPL. (b) Garnet mantle hosting intragranular trails of type II three-phase gaseous inclusions characterised by irregular shape and evidence for decrepitation. Sample EV97-45c; PPL. (c) Isolated Type III two-phase aqueous inclusions in brown amphibole. Sample EV97-45c; PPL. (d) Isolated Type IV mixed CO_2 - H_2O inclusion in Qtz from the vein. Note the negative crystal shape of the inclusion. Sample EV02-45; PPL. (e) Intragranular trails of Type V fluid inclusions (V) crosscutting a Type IV trail (IV) within Qtz from the granulitised eclogite. Sample EV02-42a; PPL. Insert: detail of Type V CO_2-rich inclusions in Qtz. Note the small amount of aqueous liquid in corners. The carbonic phase is in the vapour state. Sample EV02-45b; PPL. (f) Type VI two-phase aqueous inclusions in Qtz from the vein. Sample EV02-45; PPL.

Table 4. Representative microthermometric data of fluid inclusions in the Ama Drime eclogites. Tf = freezing temperature, Te = eutectic temperature, Ttp = triple point Tm = final melting temperature, Th = homogenisation temperature.

Sample	Host mineral	F.I. type	$TtpCO_2$ (°C)	$ThCO_2$ (°C)	Tf_{H_2O} (°C)	Te_{H_2O} (°C)	Tm_{Hhl} (°C)	Tm_{ice} (°C)	ThL_{H_2O} (°C)	Tm_{Clat} (°C)
EV97-45b/2B	Grt	I			–52.6	–28.9	–21.7	–6.6	215.8	
EV97-45b/2B	Grt	I				–29.9	–22.1	–7.2	218.7	
EV97-45b/2B	Grt	I			–45.9	–30.1	–24.1	–6.5	145.3	
EV97-45b/2B	Grt	I					–22.3		218.1	
EV97-45c/2A	Grt	II	–56.6	12.4						
EV97-45c/2A	Grt	II	–56.6	29.6						
EV97-45c/2A	Grt	II	–56.6	30.9						
EV97-45c/2A	Grt	II	–56.6	26.3						
EV97-45c/2A	Grt	II	–56.6	29.7						
EV97-45c/7B	Grt	II	–56.8	23.9						
EV97-45c/7B	Grt	II	–56.8	25.1						
EV97-45c/7B	Grt	II	–56.8	6.9						
EV97-45c/7B	Grt	II	–56.8	26.8						
EV97-45b/2D	Grt	II	–56.6	5.6						
EV97-45b/2D	Grt	II	–56.6	31.0						
EV97-45b/2E	Grt	II	–56.6	12.3						
EV02-42a/3A	Grt	II	–56.6	3.2						
EV97-45c/2C	Qtz	III			–43.0	–31.7		–2.5	207.8	
EV97-45c/2C	Qtz	III			–42.0	–31.0	–19.8	–4.2	234.5	
EV97-45c/2D	Qtz	III			–45.0			–2.7	203.5	
EV97-45c/2D	Qtz	III			–45.0	–34.2	–20.4	–2.6	182.4	8.4
EV97-45c/2D	Qtz	III			–45.0	–30.9		–2.6	214.6	
EV97-45c/3A	Qtz	III			–40.0	–29.9	–19.0	–2.5	210.7	
EV97-45c/4A	Qtz	III			–41.0	–31.8	–19.8	–2.7		
EV97-45c/5B	Qtz	III			–43.0			–1.2	168.5	
EV97-45c/5C	Qtz	III			–44.0	–32.4	–18.1	–2.1	211.1	8.2
EV97-45c/5C	Qtz	III			–40.0	–30.8	–20.4	–2.5	203.5	
EV97-45c/5D	Qtz	III			–48.0	–29.1	–21.8	–4	225.2	
EV97-45c/5E	Qtz	III			–50.0	–32.5	–20.8	–4	182.5	
EV97-45c/10A	Amp	III			–44.0		–20.0	–1.8	218.5	
EV97-45c/8A	Qtz	III			–40.4	–28.1	–18.4	–2.2		8.3
EV97-45c/6A	Qtz	III			–41.0			–1.1	165.1	
EV97-45c/6D	Qtz	III			–44.0		–20.4	–3.1	208.7	
EV97-45c/6D	Qtz	III			–44.0	–30.8	–20.4	–2.6	215.8	
EV97-45c/6D	Qtz	III			–44.0		–19.2	–2.7	153.8	
EV97-45c/12A	Qtz	IV	–56.7	30.4	–31.6					7.6
EV97-45c/11A	Qtz	IV	–56.6	28.5						8.4
EV02-45/1A	Qtz	IV	–56.6		–49.0	-33.6				9.6
EV02-45/1C	Qtz	IV	–56.4	30.9	–40.0					7.3
EV02-45/1D	Qtz	IV	–56.4	30.1			–18.3			8.4
EV02-45/1F	Ap	IV	–56.4		–46.0	–33.1		–4.6		8.1
EV02-45/1G	Qtz	IV	–56.4	30.0	–28.0			–4.2		8.2
EV02-45/1G	Qtz	IV	–56.4	30.3				–4.1		8.8
EV02-45/1E	Qtz	IV	–56.4	29.0						8.2
EV02-45/1E	Qtz	IV	–56.4	29.1						8.2
EV02-45/1E	Qtz	IV	–56.4	29.1						8.2
EV02-45/1E	Qtz	IV	–56.4	29.4						8.2
EV02-45/1E	Qtz	IV	–56.4	29.6						8.2
EV02-45/1E	Qtz	IV	–56.4	29.1						8.2
EV02-45/1E	Qtz	IV	–56.4	27.1						8.2
EV02-42a/1A	Qtz	V	–57.2							7.9
EV02-42a/1B	Qtz	V	–57.1	22.3						8.5
EV02-42a/1B	Qtz	V	–57.2	22.2						8.3
EV02-42a/1B	Qtz	V	–57.2	22.6						8.4
EV02-42a/1B	Qtz	V	–57.2	22.4						8.3
EV02-42a/1B	Qtz	V	–57.2	22.2						8.5
EV02-42a/1C	Qtz	V	–56.6							9.1
EV02-42a/1C	Qtz	V	–56.6							9.2
EV97-45c/2E	Qtz	VI			–39.0		–20.7	–0.3	374.3	
EV97-45c/7A	Qtz	VI			–42.0		–20.7	–0.7	136.3	
EV02-45/1A	Qtz	VI			–36.0		–20.7	–0.6	250.2	
EV02-45/1A	Qtz	VI			–34.0			–0.6	234.8	
EV02-45/1H	Qtz	VI			–37.0		–17.3	–0.7	299.0	
EV02-45/1H	Qtz	VI			–37.0		–17.4	–0.7	291.2	

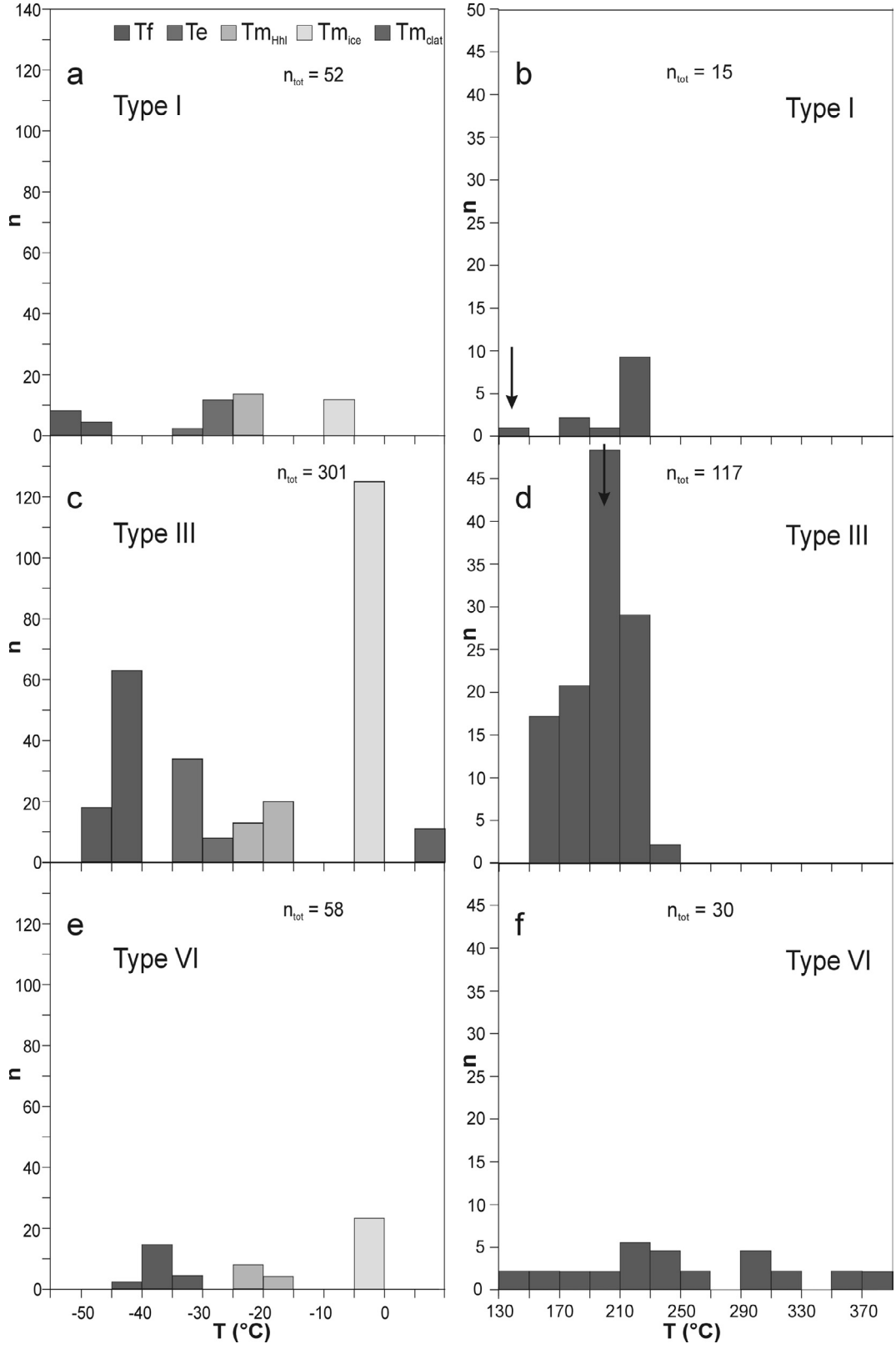

Fig. 8. Histograms for H_2O-rich fluid inclusions. (a), (c), (e) freezing (Tf), eutectic (Te), hydrohalite melting (Tm_{Hhl}), ice melting (Tm_{ice}), and clathrate melting (Tm_{clath}) temperatures for Type I, Type III, and Type VI inclusions, respectively. (b), (d), (f) homogenisation temperatures, always into the liquid (ThL_{H2O}), for Type I, Type III, and Type VI inclusions, respectively. The arrows show values selected to calculate the isochores reported in Fig. 12.

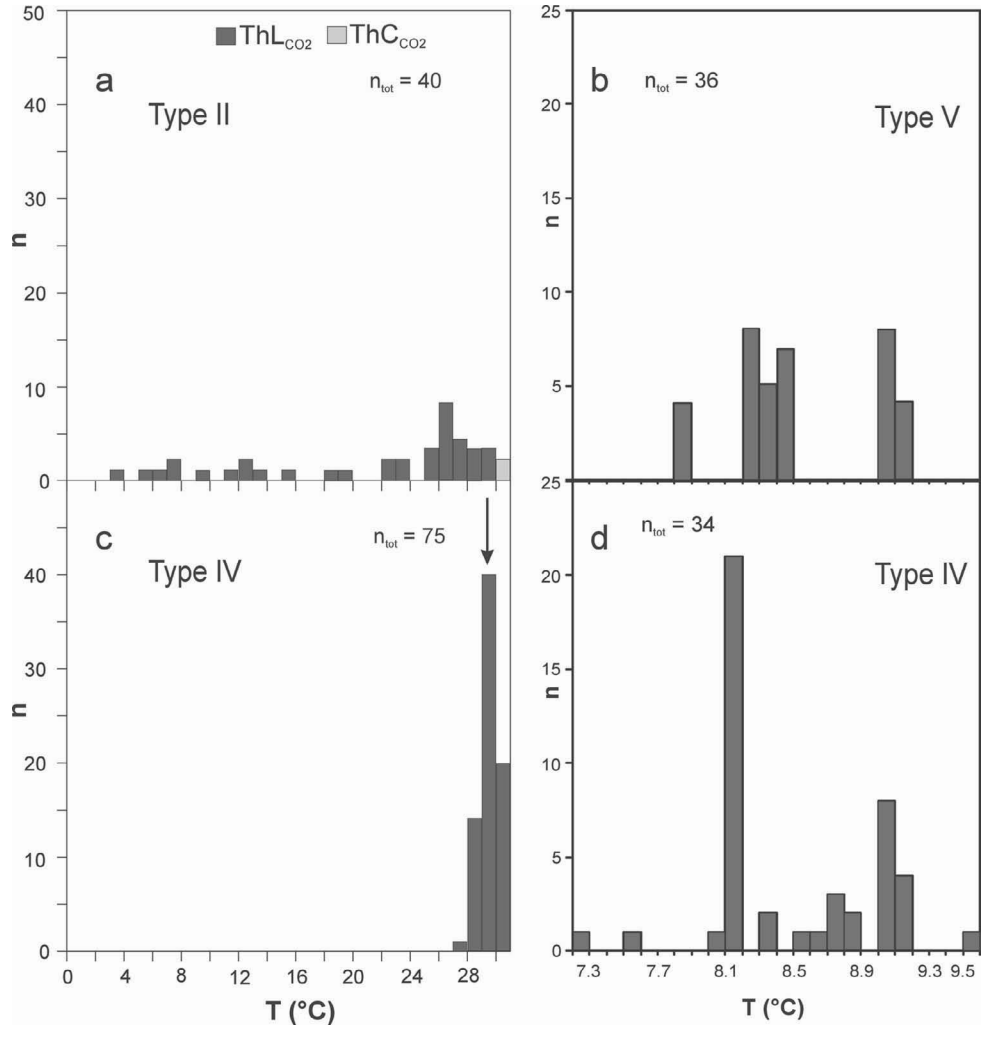

Fig. 9. Histograms for gaseous or mixed CO_2-H_2O fluid inclusions. (a), (c) homogenisation temperatures for Type II and Type IV inclusions, respectively. ThL_{CO2} = homogenisation to the liquid; ThC_{CO2} = critical homogenisation. (b), (d) clathrate melting temperatures (Tm_{clath}) for Type V and Type IV inclusions, respectively. The arrows show values selected to calculate the isochores reported in Fig. 12.

The first stage represents the pressure peak attained at eclogite-facies conditions (M1; Fig. 11). The stable mineral assemblage was garnet + omphacite + phengite + quartz + rutile, but the scarcity of eclogitic relics prevents to constrain precisely the P-T conditions. However, $P > 1.5$ GPa and $T > 580$ °C have been obtained using phase relations (stability of garnet, phengite and omphacite in the NKCFMASH+Ti system with $a_{H2O} = 0.5$) and comparing compositions of garnet cores with the X_{Ca} [Ca / (Mg + Fe + Ca) × 100] isopleths for garnet. An early decompression event ($M1_{dec}$), still at eclogite-facies conditions, led to the development of biotite + plagioclase symplectites after phengite and of clinopyroxene + plagioclase symplectites after omphacite. The topology of X_{Na} [Na / (Na + Ca) × 100] isopleths for omphacite and symplectitic clinopyroxene suggests $P < 1.8$ GPa.

The thermal peak occurred at granulite-facies conditions (stage M2, Fig. 11) and is documented by the coexistence of garnet, clinopyroxene, orthopyroxene, plagioclase and ilmenite. Phase relations and modal isopleths for orthopyroxene constrain the P-T conditions for this stage (M2) at 0.8–1.0 GPa and $T > 750$ °C, corresponding to crustal depths of about 25–30 km.

A second granulitic event (M3, Fig. 11) was responsible for the development of the Pl + Opx corona around garnet. The P-T conditions of this event were retrieved from a pseudosection calculated at $a_{H2O} = 0.5$ in the NCFMASH system to model the local equilibrium in the Pl + Opx corona. The X_{Mg} [Mg / (Mg + Fe^{2+}) × 100] isopleths for clinopyroxene and the X_{Fe} [Fe^{2+} / (Fe^{2+} + Mg) × 100] isopleths for orthopyroxene, coupled with thermobarometric data, suggest an average equilibration temperature of 783 °C at $P = 0.41$ GPa.

A first stage of cooling (M4, Fig. 11) is represented by the growth of brown amphibole in equilibrium with plagioclase, locally defining a foliation in the eclogites. The modal and compositional isopleths of amphibole and the Pl-Hbl geothermometer of Holland & Blundy (1994) indicate $T = 700$ °C, whereas the pressure is poorly constrained (0.4–0.6 GPa).

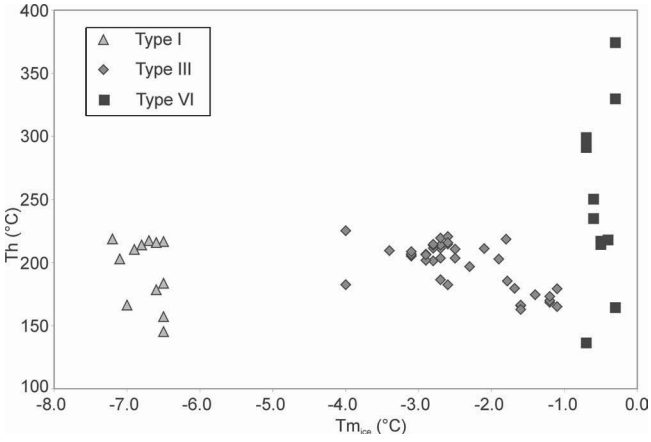

Fig. 10. Tm$_{ice}$ *versus* ThL of aqueous inclusions in granulitised eclogites from the Ama Drime range.

New minerochemical data reported in this paper reveal a late retrogression stage (M5, Fig. 11) related to the development, in sample EV02-45, of the Bt-Ap-Pl-Qtz veins cross-cutting the M4 foliation. In the host eclogite, the mineral assemblage in equilibrium with the vein is: brown biotite + green amphibole + Na-rich plagioclase. The Pl-Hbl geothermometer of Holland & Blundy (1994) suggests for stage M5 a temperature of 690 ± 7 °C for a nominal pressure of 0.4 GPa. These P-T conditions are in agreement with those inferred from garnet-biotite-sillimanite gneisses hosted in the granitic orthogneiss of the Ama Drime range ($T \approx 660$ °C and $P \approx 0.3$ GPa; Groppo *et al.*, 2007).

Evolution of the fluid phase

Textural relationships among the six GSI and the host minerals indicate that the GSI are representative of six distinct events of fluid trapping that occur at different metamorphic conditions and in different tectonic regimes. The presence of a Bt-Ap-Pl-Qtz vein adds a strong constraint to their chronology, three events occurring before the development of the vein, and three after. Figure 12 combines the P-T data for the metamorphic stages previously discussed and the fluid isochores obtained from fluid inclusion data.

The first recognised event of fluid trapping involved a high-density aqueous fluid of medium salinity and containing CO_2. This event must have occurred during subduction, at the eclogitic peak (M1 stage), as testified by the presence of primary Type I inclusions in eclogitic garnet cores. In spite of this textural evidence, the calculated isochores intersect the P-T box of the early decompression event (M1$_{dec}$; Fig. 12). Nevertheless, both the presence of daughter minerals and the asymmetric histogram obtained from homogenisation temperatures (Fig. 8b) indicate that the inclusions experienced post-trapping re-equilibrations such as shrinkage and saturation (van der Kerkhof & Hein, 2001) during exhumation. Using the highest density isochore (0.99 g/cm^3), minimum pressures of trapping are estimated to be 1.39–1.50 GPa at 750–800 °C.

Occurrence of early Type II inclusions within granulitic garnet mantles indicates the presence of pure CO_2 at the

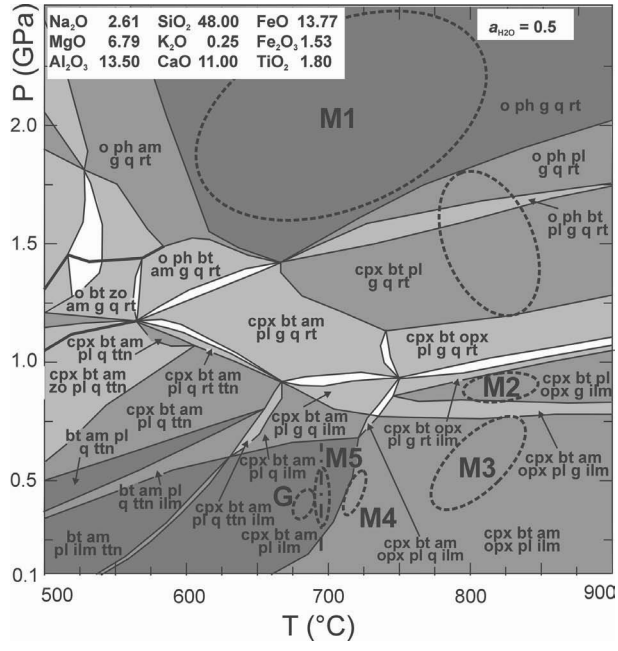

Fig. 11. P-T pseudosection for granulitised eclogite EV02-42 calculated at $a_{H2O} = 0.5$ in the NKCFMASH+Ti system, using the bulk-rock composition given in the top left inset (modified from Groppo *et al.*, 2007). White, light grey, medium grey and dark grey fields are di- tri-, quadri- and five-variant fields, respectively. Di-variant eight-phase assemblages, sharing phases of the adjacent trivariant seven-phase fields, are not labelled for clarity (am = amphibole; bt = biotite; cpx = clinopyroxene; g = garnet; ilm = ilmenite; o = omphacite; opx = orthopyroxene; ph = phengite; pl = plagioclase; q = quartz; rt = rutile; ttn = titanite; zo = zoisite). The dashed ellipses show the approximate P–T conditions for the different mineral assemblages. M1 = P–T conditions suggested by the X_{Ca} [Ca / (Mg + Fe + Ca) × 100] isopleths for garnet; early decompression = P–T conditions suggested by the X_{Na} [Na / (Na + Ca) × 100] isopleths for omphacite and clinopyroxene; M2 = P–T conditions suggested by modal isopleths of orthopyroxene; M4 = P–T conditions suggested by modal and compositional isopleths of amphibole. The P-T conditions for M3 assemblage are obtained using a pseudosection for EV02-42, calculated at $a_{H2O} = 0.5$ in the NCFMASH system, showing the X_{Mg} [Mg / (Mg + Fe^{2+}) × 100] isopleths for clinopyroxene and the X_{Fe} [Fe^{2+} / (Fe^{2+} + Mg) × 100] isopleths for orthopyroxene. M5 is the "vein-related" metamorphic stage recognised in sample EV02-45 of the present study. Dashed-dotted line is the temperature for stage M5 obtained using the Hbl-Pl geothermometer (Holland and Blundy, 1994). G is the P-T range of equilibration inferred from a garnet-biotite-sillimanite gneiss of the Ama Drime range (Groppo *et al.*, 2007).

thermal peak (stage M2), during the first stage of decompression. Unfortunately, pressure conditions for trapping obtained from the calculated isochores are inconsistent with the P conditions of this first granulite-facies event (Fig. 12). In fact, even the highest density isochore (0.91 g/cm^3) gives pressures compatible only with the stages from M3 to the greenschist-facies event (M5). This is due to post-trapping re-equilibrations, as testified by the presence of daughter minerals in the Type II fluid inclusions and by the asymmetric histogram for Th.

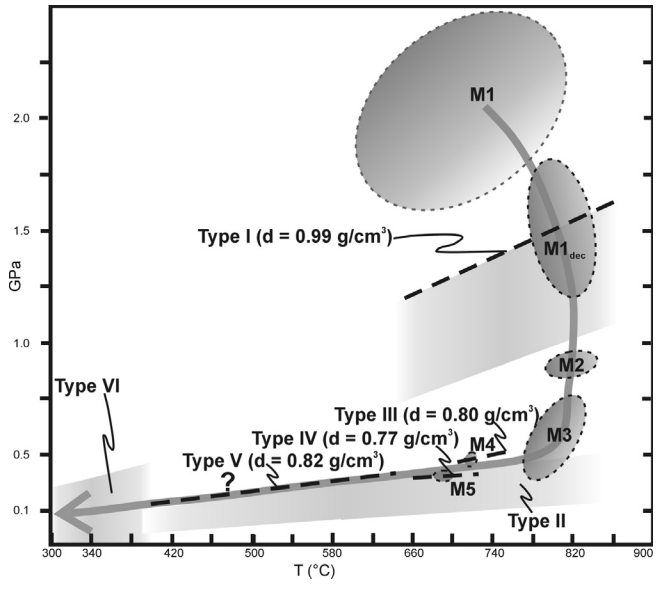

Fig. 12. comparison between fluid inclusion isochores and the P-T path estimated for the granulitised eclogites and associated vein from Ama Drime range. M1 – M5 are the metamorphic stages for the eclogite reported in Fig. 11. To simplify the figure, maximum and minimum densities are reported only for Type I, Type II and Type VI fluid inclusions (light grey fields). Dashed lines are the representative isochores obtained from Type I, Type III, and Type V fluid inclusions. The dark grey arrow is the inferred P-T path.

The last fluid influx experienced by the granulitised eclogites before the development of the Bt-Ap-Pl-Qtz vein is represented by a low-salinity - low-density aqueous fluid. The occurrence of primary fluid inclusions in brown amphibole indicates that this fluid is responsible of the rock hydration during stage M4. The preserved density of trapping in the fluid inclusions, testified by the symmetric distribution of Th, gives a tight constraint to the pressure conditions of this stage, previously only loosely constrained at 0.4–0.6 GPa by the P-T pseudosection of Groppo *et al.*, (2007). In fact, for a temperature of 720 °C a pressure of about 0.47 GPa is obtained by the calculated isochore (Fig. 12).

The fluid responsible for the development of the Bt-Ap-Pl-Qtz vein cross-cutting the foliation is a homogeneous, low-density, aqueo-carbonic fluid. Textural relationships between the vein and the host eclogite, i.e. the strong retrogression of the eclogite at the contact with the vein, indicate that this fluid is also responsible of the late stage of retrogression (M5). The isochore calculated using the Th corresponding to the peak of the symmetric histogram (Fig. 8d) constrains the pressure of stage M5 at about 0.39 GPa, for a temperature of 700 °C (Fig. 12).

The fifth event observed is the entrapment of a homogeneous CO_2-rich fluid with low salinity and low density. Textural relationships suggest that this fluid was trapped after the low-density aqueo-carbonic fluid (Type IV) and before the entrapment of very-low salinity aqueous fluid (Type VI), i.e. at P-T conditions between 0.37 GPa at 650 °C and 0.14 GPa at 400 °C (Fig. 12). Unfortunately, no metamorphic mineral assemblage is apparently associated with this fluid influx and in this P-T range a fluid with Type V composition is always miscible (*e.g.* Diamond, 2003). These characteristics prevent from precisely constraining the T and P conditions of the trapping event.

The last fluid trapped is an aqueous fluid with very-low salinity, probably representative of low pressure and low temperature conditions (Fig. 12). The absence of a greenschist-facies mineral assemblage and the scattered Th obtained from Type VI fluid inclusions preclude any precise constraint on the P-T conditions for this trapping event.

Origin of the fluid phase

The data obtained by this fluid inclusion study are not in themselves sufficient to define the origin of the different fluids observed in the Ama Drime eclogites. However, comparing these data with those obtained from other localities of the Himalayas and from other collisional orogens, it is possible to discuss different hypotheses.

Few data are reported in the geological literature about the nature of metamorphic fluids during subduction of continental crust and the early stages of its exhumation in the Himalayan orogen. The only available data on HP fluids are from the Tso-Morari eclogites, where an aqueous fluid of medium salinity (11–13 wt % $NaCl_{eq}$) is in equilibrium with the HP mineral assemblage (Sachan *et al.*, 1999). We found that the fluid in equilibrium at the eclogitic peak in the Ama Drime granulitised eclogites is an aqueous fluid characterised by medium salinity and containing CO_2. The nature of the fluids trapped at HP conditions in both the western Himalayan (Tso-Morari) eclogites and eastern Himalayan (Ama Drime) eclogites is consistent with the aqueous-dominated system observed at eclogite-facies conditions in other continental rocks from orogens of different ages (Philippot *et al.*, 1995; Scambelluri *et al.*, 1998; Xiao *et al.*, 2000; Fu *et al.*, 2002; Ferrando *et al.*, 2005). The origin of peak fluid in the Ama Drime eclogites, however, remains uncertain. Data from continental lithologies suggest fluid segregation and limited fluid transport during eclogite-facies conditions (i.e. an internal origin for the eclogitic fluids; Nadeau *et al.*, 1993; Klemd & Bröcker, 1999; Touret & Frezzotti, 2003; Frezzotti *et al.*, 2004 and references therein).

According to Lombardo & Rolfo (2000), the eclogites of the Ama Drime range derive from discordant mafic dykes emplaced in the granitic protolith of the orthogneiss. Geochemically, they have an olivine-tholeiitic composition and may derive from Fe-rich dolerites, possibly related to the Cretaceous Rajmahal Trap volcanism widespread in NE India (Rolfo *et al.*, 2005). Because of the scarce mobility of the fluid at HP conditions, the eclogitic fluids may represent remnants of fluids internally buffered during late stages of prograde metamorphism (Fig. 13).

In contrast with the mineral assemblage developed at the HP peak, the granulite-facies mineral assemblage formed in the first stage of decompression is in equilibrium with pure CO_2, i.e. the fluid found in most granulites (*e.g.* Andersen *et al.*, 1990; Munyanyiwa *et al.*, 1993; Touret, 1995;

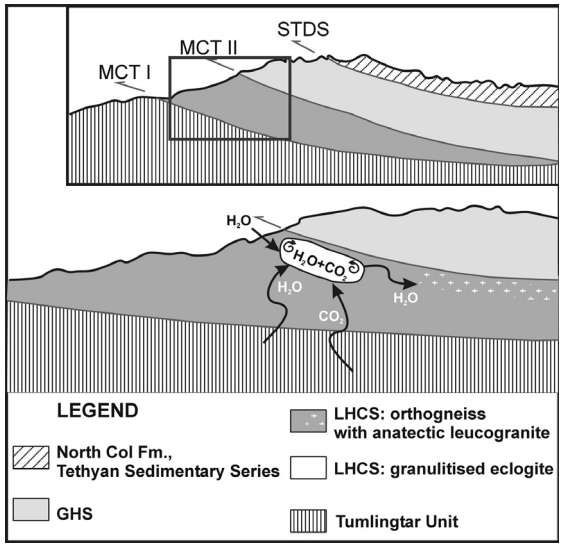

Fig. 13. Cartoon illustrating possible sources of the fluids found in the granulitised eclogites from the Ama Drime range. MCT = Main Central Thrust; STDS = South Tibetan Detachement System; GHS = Greater Himalayan Sequence; LHCS = Lesser Himalayan Crystalline Sequence.

Klemd & Brocker, 1999; Touret & Frezzotti, 2003) as well as in eclogites that experienced granulite-facies overprint (*e.g.* Fu *et al.*, 2003). As concerning the "granulitic" CO_2, the major question does not regard its origin (juvenile or sedimentary; Touret, 1986), but the processes that introduced CO_2 in the system during granulitisation, namely mantle-derived intrusions, metamorphic reactions (*e.g.* decarbonation reactions, graphite oxydation), and/or preferential incorporation of H_2O in anatectic melts (see Touret & Frezzotti, 2003; Frezzotti *et al.*, 2004 and references therein). A direct influx of CO_2 rising from mantle-derived intrusions is unlikely in the case of the Ama Drime eclogites because there is no direct evidence of this kind of intrusions in the studied area. The hypothesis of a CO_2 influx from metamorphic reactions in nearby sediments is unsuitable either, because the LHCS in the studied area (i.e. the Ama Drime orthogneiss) does not include marbles or carbonaceous sediments and the structurally lower metasedimentary Tumlingtar Unit is inferred to be emplaced below the LHCS after the stage M2 (see later on). On the contrary, field and petrologic evidence (Lombardo & Rolfo, 2000; Groppo *et al.*, 2007) suggests that the eclogite and country rocks experienced the same metamorphic evolution. In particular, the orthogneiss shows evidence of partial melting (Fig. 3b) that can be ascribed to the thermal peak (stage M2) attained during the first stages of decompression, possibly through dehydration melting of white mica (*e.g.* Indares & Dunning, 2001). Natural and experimental observations indicate that H_2O is preferentially partitioned into the granitic melt and, as a consequence, CO_2 concentrates in the residual fluid (*e.g.* Holloway, 1976; Touret & Dietvorst, 1983; Touret & Olsen, 1985; Holtz *et al.*, 2001). For these reasons, the most likely process to produce "granulitic" CO_2 in the Ama Drime eclogite may be preferential incorporation of H_2O into the melts produced during anatexis of the hosting gneiss. Specifically, the loss of H_2O from the peak aqueous fluid containing CO_2 to the hosting migmatites during stage M2 may have caused CO_2 enrichment in the residual fluid of the eclogites (Fig. 13).

The LP-M/HT stage M4 is dominated by aqueous fluids. The growth of oriented brown amphibole testifies pervasive retrogression probably associated to a regional deformation event. This suggests a considerable influx of external aqueous fluids connected to a tectonic event. As already mentioned, geologic evidence (Meier & Hiltner, 1993; Goscombe & Hand, 2000) suggests that tectonic coupling of the LHCS with the underlying metasedimentary Tumlingtar Unit probably occurred during or after our stage M4, following a tectonic event responsible of the development of the main foliation. The downward heat conduction from the hot LHCS onto the cold Tumlingtar Unit is considered the cause of prograde metamorphism recorded in the latter (Meier & Hiltner, 1993; Pognante & Benna, 1993). Prograde dehydration reactions in this Unit may be the source of the Type III aqueous fluid (Fig. 13). It is interesting to note that the occurrence of an aqueous fluid in equilibrium with the amphibolite-facies mineral assemblage defining the main schistosity is widespread in the Annapurna region of the Nepal Himalaya (Pêcher, 1978; Pêcher, 1979; Craw, 1990).

An influx of aqueo-carbonic fluids during an extensional event (stage M5) caused both vein formation and strong retrogression of the eclogite. A similar fluid was also reported by previous authors in "late" veins and segregations from the western and central Himalaya (Leroy *et al.*, 1975; Pêcher, 1979; Sauniac & Touret, 1983; Craw, 1990; Boullier *et al.*, 1991; Morrison & Oliver, 1993; Sachan *et al.*, 2001; Pandey & Virdi, 2003; Pandey *et al.*, 2004; Carosi *et al.*, 2005). The origin of this fluid may be the same invoked for Type III fluid inclusions, i.e. mixing of CO_2 and H_2O released from prograde reactions in the underlying Tumlingtar Unit (Fig. 13). In fact, the metasedimentary Tumlingtar Unit contains also carbonatic phyllites and dolomite marbles (Andrews, 1985; Meier & Hiltner, 1993). In addition to dehydration reactions, the progressive increase of temperature during metamorphism may have induced decarbonation reactions in these lithologies. Such an origin is in agreement with stable isotope data collected on minerals and CO_2-H_2O fluid inclusions in quartz lenses from the Annapurna region, that suggest fluid percolation from nearby formations (Boullier *et al.*, 1991) and are an evidence in favour of a Le Fort (1975)-type model for the Himalayan inverse metamorphism, with cooling of the MCT hanging wall and conductive heating of the footwall. Similarly, the presumed origin for CO_2 in H_2O-CO_2 fluids found in quartz veins from the Kathmandu Klippe is from metamorphic reactions involving the underlying carbonate- and graphite-rich Benighat Slates (Morrison & Oliver, 1993). Besides, other authors relate the influx of CO_2-H_2O fluids in central Himalaya with metamorphic reactions that produced degassing during movement along the MCT (*e.g.* Pêcher, 1978; Sachan *et al.*, 2001; Kerrick & Caldeira, 1999). A similar origin is also suggested for the CO_2-H_2O fluid trapped at amphibolite–facies conditions in

quartzite in the footwall of the Jakhri Thrust Zone, NW Himalaya (Pandey & Virdi, 2003; Pandey *et al.*, 2004).

Type V CO_2-rich fluid found in both the eclogite and vein may derive from the same source. The high amount of CO_2 in the fluid may be due to an increase of CO_2 and/or a decrease of H_2O influx from the underlying Tumlingtar Unit.

The last fluid that percolated through the granulitised eclogites was an aqueous fluid. It is probably related to percolation of meteoric water at shallow levels (Fig. 13), as usually observed in western and central Himalaya (Leroy *et al.*, 1975; Pêcher, 1978; Sauniac & Touret, 1983; Craw, 1990; Boullier *et al.*, 1991; Kerrick & Caldeira, 1999; Sachan & Mukherjee, 2001; Sachan *et al.*, 2001; Pandey & Virdi, 2003; Pandey *et al.*, 2004) and world-wide in metamorphic rocks (Yardley *et al.*, 2000).

Conclusions

This fluid inclusion study has described, for the first time in the Himalayan orogen, the evolution of the fluid phase in continental rocks along a clockwise loop from HP-peak conditions during subduction to metamorphic T-peak during decompression and the to MT-LP conditions during late stages of exhumation. The fluid phase evolution is complex, but compatible with the P-T path of the Ama Drime granulitised eclogites retrieved from microstructural data, P-T pseudosections and conventional thermobarometry (Groppo *et al.*, 2007). Such P-T path is characterised by strong decompression (from 1.5–1.6 GPa to 0.4–0.5 GPa) at high T, followed by nearly isobaric cooling from 750 °C to 400 °C at low P. The low a_{H2O} responsible for the growth of the anhydrous mineral assemblage during the granulitic stage M2 is related to the presence of pure CO_2 in the system caused by preferential adsorption of H_2O by granitic partial melts in the host orthogneiss. Similarly, the influx of aqueous fluids at LP-H/MT conditions produced an increase of a_{H2O} and was responsible for the growth of hydrous minerals during stage M4. The aqueous nature of the fluid phase at the eclogitic peak (stage M1) is consistent with that reported at HP conditions in eclogites from the western Himalaya (Tso-Morari; Sachan *et al.*, 1999), though these eclogites experienced a different post-peak evolution (i.e. decompression under decreasing temperatures in contrast to nearly isothermal decompression in the eastern Himalaya eclogites). Also the presence of mixed H_2O-CO_2 fluids during amphibolite-facies conditions (stage M5) is commonly reported in both western and central Himalaya (*e.g.* Morrison & Oliver, 1993; Pandey *et al.*, 2004). On the other hand, the Ama Drime eclogites do not show evidence for the fluid immiscibility found in the Nanga Parbat (*e.g.* Poage *et al.*, 2000) and Namche Barwa (Craw *et al.*, 2005) syntaxes that is clearly related to recent and rapid uplift.

From a tectonic viewpoint, both fluid and metamorphic evolutions suggest that the Ama Drime rocks, like the Tso-Morari eclogites, experienced HP metamorphism during subduction of Indian continental crust, though probably at lesser P. Unlike the Tso-Morari eclogites, where strong evidence of decompression under decreasing temperatures suggests exhumation along a cooling path, possibly by thrusting associated with accretion of the metamorphic pile onto the base of the overriding plate, the Ama Drime eclogites ponded at intermediate crustal levels and were subjected to thermal relaxation and consequent strong granulite-facies overprinting. Further decompression exhumed the granulitised eclogites at shallow crustal levels, where these rocks were partly hydrated to amphibolites and finally isobarically cooled.

Acknowledgements: The authors are grateful to C. Groppo for constructive discussions. M.L. Frezzotti is thanked for microRaman analysis. C. Sibio made the thick sections for fluid inclusion study. The manuscript was constructively reviewed by D. Craw and an anonymous review. Useful comments of R. Klemd are gratefully acknowledged. This work was supported by C.N.R. Institute of Geosciences and Georesources and by P.R.I.N. Cofin 2003. Raman analytical facilities in Siena were provided by the Italian Program for Research in Antarctica (P.N.R.A.).

References

Andersen, T., Austrheim, H., Burke, E.A.J. (1990): Fluid inclusions in granulites and eclogites from the Bergen Arcs, Caledonides of W. Norway. *Mineral. Mag.*, **54**, 145-158.

Andrews, E. (1985): Stratigraphy of the Sabhaya Khola region, Sankhuwa Sabha district, eastern Nepal. *J. Nepal Geol. Soc.*, **2**, 12-35.

Arita, K. (1983): Origin of the inverted metamorphism of the Lower Himalayas, Central Nepal. *Tectonophysics*, **93**, 43-60.

Bakker, R.J. (1997): CLATHRATES: computer programs to calculated fluid inclusion V-X properties using clathrate melting temperatures. *Computers & Geosciences*, **23**, 1-18.

— (2003): Package FLUIDS 1. Computer programs for analysis of fluid inclusion data and for modelling bulk fluid properties. *Chem. Geol.*, **194**, 3-23.

Bakker, R.J. & Brown, P. (2003): Computer modelling *in* fluid inclusion research. *in* Fluid inclusions: analysis and interpretation, I. Samson, A. Anderson, D. Marshall, eds. Mineral. Assoc. Can., Short Course Series, **32**, 175-212.

Bordet, P. (1961): Recherches géologiques dans l'Himalaya du Népal, région du Makalu. *Editions du Centre National de la Recherche Scientifique*, Paris, 275 pp.

Borghi, A., Castelli, D., Lombardo, B., Visonà, D. (2003): Thermal and baric evolution of garnet granulites from the Kharta region of S Tibet, E Himalaya. *Eur. J. Mineral.*, **15**, 401-418.

Boullier, A.M., France-Lanord, C., Dubessy, J., Adamy, J., Champenois, M. (1991): Linked fluid and tectonic evolution in the High Himalaya mountains (Nepal). *Contrib. Mineral. Petrol.*, **107**, 358-372.

Brunel, M. (1983): Etude pétro-structurale des chevauchements ductiles en Himalaya (Népal oriental et Himalaya du Nord– Ouest). Thèse Doct. Sciences, Université de Paris VII, 395.

Burchfiel, B. C., Chen, Z., Hodges, K. V., Yuping, L., Royden, L. H., Changrong, D., Jiene, X. (1992): The south Tibetan detachment system, Himalayan Orogen: extension contemporaneous

with and parallel to shortening in a collisional mountain belt. *Geol. Soc. Am. Spec. Pap.*, **269**, 41.

Bureau of Geology and Mineral Resources of Xizang Autonomous Region (1993): Regional geology of Xizang (Tibet) Autonomous Region. People's Republic of China, Ministry of Geology and Mineral Resources, Geological Publishing House, Beijing, Geological Memoirs, ser. 1, 31, 707 (in Chinese, with English summary).

Burg, J.P. (1983): Tectogénèse comparée de deux segments de chaînes de collision: le sud du Tibet et la Chaîne Hercynienne d'Europe. Thèse d'Etat, Université des Sciences et Techniques du Languedoc, Montpellier, 361.

Burg, J.P., Brunel, M., Gapais, D., Chen, G., Liu, G. (1984): Deformation of leucogranites in the crystalline Main Central Sheet in southern Tibet (China). *J. Struct. Geol.*, **6**, 535-542.

Carosi, R., Lombardo, B., Molli, G., Musumeci, G., Pertusati, P.C. (1998): The south Tibetan detachment system in the Rongbuk Valley, Everest region. Deformation features and geological implications. *J. Asian Earth Sci.*, **16**, 299-311.

Carosi, R., Montomoli, C., Ruggieri G. (2005): Tectonic evolution and fluid inclusion data of the Main Central Thrust Zone in the Lower Dolpo (Western Nepal). European Current Research On Fluid Inclusions (ECROFI XVIII), Siena, Italy, 6–9 July 2005, Abstract CD.

Connolly, J.A.D. (1990): Multivariable phase diagrams: an algorithm based on generalized thermodynamics. *Am. J. Sci.,* **290,** 666-718.

Cottle, J.M, Jessup, M.J., Newell, D.L., Searle, M.P., Law, R.D. (2006): Structure of the South Tibetan Detachment System, Kharta region south Tibetan Himalaya. *J. Asian Earth Sci.*, **26**, 132.

Craw, D. (1990): Fluid evolution during uplift of the Annapurna Himal, Central Nepal. *Lithos*, **24**, 137-150.

Craw, D., Koons, P.O., Winslow, D., Chamberlain, C.P., Zeitler, P. (1994): Boiling fluids in a region of rapid uplift, Nanga Parbat Massif, Pakistan. *Earth Planet. Sci. Lett.*, **128**, 169-182.

Craw, D., Chamberlain, C.P., Zeitler, P.K., Koons, P.O. (1997): Geochemistry of a dry steam geothermal zone formed during rapid uplift of Nanga Parbat, northern Pakistan. *Chem. Geol.*, **142**, 11-22.

Craw, D., Koons, P.O., Zeitler, P.K., Kidd, S.F. (2005): Fluid evolution and thermal structure in the rapidly exhuming gneiss complex of Namche Barwa-Gyala Peri, eastern Himalayan syntaxis. *J. Metamor. Geol.*, **23**, 829-845.

Diamond, L.W. (2003): Introduction to gas-bearing, aqueous fluid inclusions. *in* Fluid inclusions. Analysis and interpretation, I. Samson, A. Anderson, D. Marshall, eds. Mineralogical Association of Canada, Short Course Series, **32**, 101-158.

Dietrich, V. & Gansser, A. (1981): The leucogranites of the Bhutan Himalaya (crustal anatexis versus mantle melting). *Schweiz. Mineral. Petrogr. Mitt.*, **61**, 177-202.

Ferrando, S., Frezzotti, M.L., Dallai, L., Compagnoni, R. (2005): Fluid-rock interaction in UHP phengite-kyanite-epidote eclogite from the Sulu orogen, Eastern China. *Int. Geol. Rev.*, **47**, 750-774.

Ferrara, G., Lombardo, B., Tonarini, S. (1983): Rb/Sr Geochronology of Granite and Gneisses from the Mount Everest Region, Nepal Himalaya. *Geol. Rundschau*, **72**, 119-136.

Frezzotti, M.L., Cesare, B., Scambelluri, M. (2004): Fluids at extreme P-T metamorphic conditions: the message from high-grade rocks. *Periodico di Mineralogia*, special issue 2: A showcase of the Italian research in metamorphic petrology, **73**, 209-219.

Fu, B., Zheng, Y.-F., Touret, J.L.R. (2002): Petrological, isotopic and fluid inclusion studies of eclogites from Sujiahe, NW Dabie Shan (China). *Chem. Geol.*, **187**, 107-128.

Fu, B., Touret, J.L.R., Zheng, Y.-F., Jahn, B.-M. (2003): Fluid inclusions in granulites, granulitized eclogites and garnet clinopyroxenites from the Dabie-Sulu terranes, eastern China. *Lithos*, **70**, 293-319.

Goscombe, B., Hand, M. (2000): Contrasting P-T paths in the eastern Himalaya, Nepal: inverted isograds in a paired metamorphic mountain belt. *J. Petrol.*, **41**, 1673-1719.

Groppo, C., Lombardo, B., Rolfo, F., Pertusati, P. (2007): Clockwise exhumation path of granulitized eclogites from the Ama Drime range (Eastern Himalayas). *J. Metamor. Geol.,* **25**, 51-75.

Hodges, K.V., Bowring, S., Davidek, K., Hawkins, D., Krol, M. (1998): Evidence for rapid displacement on Himalayan normal faults and the importance of tectonic denudation in the evolution of mountain ranges. *Geology*, **26**, 483-486.

Holland, T.J.B., Blundy, J.D. (1994): Non-ideal interactions in calcic amphiboles and their bearing on amphibole-plagioclase thermometry. *Contrib. Mineral. Petrol.*, **116**, 433-447.

Holloway, J.R. (1976): Fluids in the evolution of granitic magmas: consequences of finite CO_2 solubility. *Geol. Soc. Am. Bull.*, **87**, 1513-1518.

Holtz, F., Johannes, W., Tamic, N., Behrens, H. (2001): Maximum and minimum water contents of granitic melts generated in the crust: a re-evaluation and implications. *Lithos*, **56**, 1-14.

Indares, A. & Dunning, G. (2001): Partial melting of high-P-T metapelites from the Tshenukutish Terrane (Grenville Province): petrography and U-Pb geochronology. *J. Petrol.*, **42**, 1547-1565.

Kerrick, D.M., Caldeira, K. (1999): Was the Himalayan orogen a climatically significant couplet source and sink for atmospheric CO_2 during the Cenozoic?. *Earth Planet. Sci. Lett.*, **173**, 195-203.

Klemd, R., Bröcker, M. (1999): Fluid influence on mineral reactions in ultrahigh-pressure granulites: a case study in the Snieznik Mts. (West Sudetes, Poland). *Contrib. Mineral. Petrol.*, **136**, 358-373.

Kretz, R. (1983): Symbols for rock-forming minerals. *Am. Mineral.*, **68**, 277-279.

Le Fort, P. (1975): Himalaya: the collided range: Present knowledge of the continental arc, *Am. J. Sci.*, **275A**, 1-44.

Leake, B.E., Woolley, A.R., Birch, W.D., Burke, E.A.J., Ferraris, G., Grice, J.D., Hawthorne, F.C., Kisch, H.J., Krivovichev, V.G., Schumacher, J.C., Stephenson, N.C.N., Whittaker, E.J.W. (2004): Nomenclature of amphiboles: additions and revisions to the International Mineralogical Association's amphibole nomenclature. *Eur. J. Mineral.*, **16**, 191-196.

Leroy, J., Le Fort, P., Poty, B. (1975): Some quartz crystals and their fluid inclusions from the Nepal Himalaya. *Himalayan Geol.*, **5**, 139-152.

Li, D., Liao, Q., Yuan, Y., Wan, Y., Liu, D., Zhang, X., Yi, S., Cao, S., Xie, D. (2003): SHRIMP U-Pb zircon geochronology of granulites at Rimana (Southern Tibet) in the central segment of Himalayan Orogen. *Chinese Science Bulletin,* **48**, 2647-2650.

Liu, S., Zhang, J., Shu, G., Li, Q. (2005): Mineral chemistry, P-T-t paths and exhumation processes of mafic granulites in Dinggye, Southern Tibet. *Science in China Ser. D Earth Sciences*, **48/11,**

1870-1881.

Liu, Y., Siebel, W., Massonne, H.-J., Xiao, X. (2007): Geochronological and petrological constraints for tectonic evolution of the Central Greater Himalayan Sequence in the Kharta area, Southern Tibet. *J. Geol.*, **115**, 215-230.

Lombardo, B. & Rolfo, F. (2000): Two contrasting eclogite types in the Himalayas: implications for the Himalayan orogeny. *J. Geodynam.*, **30**, 37-60.

Lombardo, B., Pertusati, P., Borghi, A. (1993): Geology and tectono-magmatic evolution of the eastern Himalaya along the Chomolungma-Makalu transect. *in* Himalayan Tectonics, P.J. Treloar & M.P. Searle, eds. Geological Society of London, Special Publication, **74**, 341-355.

Lombardo, B., Pertusati, P., Rolfo, F., Visonà, D. (1998): First report of eclogites from the E Himalaya: implications for the Himalayan orogeny. *Mem. Sci. Geol.*, **50**, 67-68.

Meier, K. & Hiltner, E. (1993): Deformation and metamorphism within the Main Central Thrust zone, Arun tectonic Window, eastern Nepal. *in* Himalayan Tectonics, P.J. Treloar & M.P. Searle, eds. Geological Society of London, Special Publication, **74**, 541-558.

Morimoto, N. (1988): Nomenclature of pyroxenes. *Mineral. Mag.*, **52**, 535-550.

Morrison, C.W.K. & Oliver, G.J.H. (1993): A study of illite crystallinity and fluid inclusions in the Kathmandu Klippe and the Main Central Thrust znoe, Nepal. *in* Himalayan Tectonics, P.J. Treloar, M.P. Searle, eds. Geological Society Special Publication, **74**, 525-540.

Munyanyiwa, H., Touret, J.L.R., Jelsma, H.A. (1993): Thermobarometry and fluid evolution of enderbites within the Magondi Mobile Belt, northern Zimbabwe. *Lithos*, **29**, 163-176.

Murphy, M. & Harrison, T.M. (1999): Relationship between leucogranites and the Qomolangma detachment in the Rongbuk Valley, South Tibet. *Geology*, **27**, 831-837.

Nadeau, S., Philippot, P., Pineau, F. (1993): Fluid inclusion and mineral isotopic compositions (H-C-O) in eclogitic rocks as tracers of local fluid migration during high-pressure metamorphism. *Earth Planet. Sci. Lett.*, **114**, 431-448.

Pandey, A.K. & Virdi, N.S. (2003): Microstructural and fluid inclusion constraints on the evolution of Jakhri Thrust Zone in the Satluj valley of NW Himalaya. *Curr. Sci.*, **84**, 1355-1364.

Pandey, A.K., Sachan, H.K., Virdi, N.S. (2004): Exhumation history of a shear zone constrained by microstructural and fluid inclusion techniques: an example from the Satluj valley, NW Himalaya, India. *J. Asian Earth Sci.*, **23**, 391-406.

Pêcher, A. (1978): Deformation et metamorphisme associés a une zone de cisallement. Example du grand chevauchement central Himalayen (MCT), transversale des Annapurnas et du Manaslu, Népal. Thèse Doct. Sciences, Université de Grenoble, 353.

— (1979): Les inclusions fluides des quartz d'exsudation de la zone du M.C.T. hamalayen au Népal central: Données sur la phase fluide dans une grande zone de cisaillement crustal. *Bull. Minéral.*, **102**, 537-554.

Philippot, P., Chevallier, P., Chopin, C., Dubessy, J. (1995): Fluid composition and evolution in coesite-bearing rocks (Dora-Maira massif, Western Alps): implications for element recycling during subduction. *Contrib. Mineral. Petrol.*, **121**, 29-44.

Poage, M.A., Page Chamberlain, C., Craw, D. (2000): Massif-wide metamorphism and fluid evolution at Nanga Parbat, Northern Pakistan. *Am. J. Sci.*, **300**, 463-482.

Pognante, U. & Benna, P. (1993): Metamorphic zonation, migmatization, and leucogranites along the Everest transect (Eastern Nepal and Tibet): record of an exhumation history. *in* Himalayan Tectonics, P.J. Treloar & M.P. Searle, eds. Geol. Soc. Spec. Publ, **74**, 323-340.

Pouchou, J.L. & Pichoir, F. (1988): Determination of mass absorption coefficients for soft X-Rays by use of the electron microprobe. *Microbeam Analysis*, San Francisco Press, 319-324.

Raase, P. (1974): Al and Ti contents of hornblende, indicators of pressure and temperature of regional metamorphism. *Contrib. Mineral. Petrol.*,**45**, 231-236.

Robinson, D., DeCelles, P.G., Patchett, J., Garzione, C.N. (2001): The kinematic evolution of the Nepalese Himalaya interpreted from Nd isotopes. *Earth Planet. Sci. Lett.*, **192**, 507-521.

Roedder, E. (1984): Fluid inclusions. *Rev. Mineral.*, Mineral. Soc. Am., **12**, 678.

Rolfo, F., Lombardo, B., Mcclelland, W. (2005): Geochemistry and geochronology of E Himalaya Eclogites. *Mitt. Österr. Miner. Ges.* **150,** 134.

Sachan, H.K. & Mukherjee, B.K. (2001): Evidences of fluid re-equilibration in blueschist rocks from Shergol Ophiolitic Melange, Indus Suture Zone, Ladakh. *Himalayan Geol.*, **22**, 127-133.

Sachan, H.H., Bodnar, R.J., Islam, R., Szabó, C., Law, R.D. (1999): Exhumation history of eclogites from the Tso-Morari Crystalline Complex in Eastern Ladakh: mineralogical and fluid inclusion constraints. *J. Geol. Soc. India*, **53**, 181-190.

Sachan, H.K., Sharma, R., Sahai, A., Gururajan, N.S. (2001): Fluid events and exhumation history of the main central thrust zone Garhwal Himalaya (India). *J. Asian Earth Sci.*, **19**, 207-221.

Sauniac, S. & Touret, J.L.R. (1983): Petrology and fluid inclusions of a quartz-kyanite segregation in the main thrust zone of the Himalayas. *Lithos*, **16**, 35-45.

Scambelluri, M., Pennacchioni, G., Philippot, P. (1998): Salt-rich aqueous fluids formed during eclogitization of metabasites in the Alpine continental crust (Austroalpine Mt. Emilius unit, Italian western Alps). *Lithos*, **43**, 151-167.

Schärer, U. (1984): The effect of initial ^{230}Th disequilibrium on young U-Pb ages; the Makalu case, Himalaya. *Earth Planet. Sci. Lett.*, **67**, 191-204.

Schärer, U., Xu, R., Allegre, C.J. (1986): U-(Th)-Pb systematics and ages of Himalayan leucogranites, South Tibet. *Earth Planet. Sci. Lett.*, **77**, 35-48.

Simpson, R.L., Parrish, R.R., Searle, M.P., Waters, D.J. (2000): Two episodes of monazite crystallization during metamorphism and crustal melting in the Everest region of the Nepalese Himalaya. *Geology*, **28**, 403-406.

Touret, J.L.R. (1986): Fluid inclusions in rocks from the lower continental crust. *in* The nature of the lower continental crust, J.B. Dawson, D.A. Carswell, J. Hall, K.H. Wedepohl, eds. Geological Society Special Publication, **24**, 161-172.

—, (1995): The role and nature of fluids in the continental lower crust. India and Antarctica during the Precambrian, *Mem. Geol. Soc. India*, **34**, 143-160.

—, (2001): Fluids in metamorphic rocks. *Lithos*, **55**, 1-25.

Touret, J.L.R. & Dietvorst, P. (1983): Fluid inclusions in high-grade anatectic metamorphites. *J. Geol. Soc. London*, **140**, 635-649.

Touret, J.L.R. & Frezzotti, M.L. (2003): Fluid inclusions in high pressure and ultrahigh pressure metamorphic rocks. *in* Ultrahigh-pressure metamorphism, D.A. Carswell & R. Compagnoni, eds. E.M.U. Notes in Mineralogy, **5**, 467-487.

Touret, J.L.R. & Olsen, S. N. (1985): Fluid inclusions in migmatites. *in* Migmatites, J. R. Ashworth, ed. Blakie Publication, 265-286.

Ulmer, P. (1986): NORM-Program for cation and oxygen mineral norms. Computer Library, Institut fûr Mineralogie und Petrographie, ETH-Zentrum, Zürich, Switzerland.

Upreti, B.N. (1999): An overview of the stratigraphy and tectonics of the Nepal Himalaya. *J. Asian Earth Sci.*, **17**, 577-606.

Xiao, Y.L., Hoefs, J., van den Kerkhof, A.M., Fiebig, J., Zheng, Y. (2000): Fluid history of UHP metamorphism in Dabie Shan, China: a fluid inclusion and oxygen isotope study on the coesite-bearing eclogite from Bixiling. *Contrib. Mineral. Petrol.*, **139**, 1-16.

Vannay, J.C., Grasemann, B., Rahn, M., Frank, W., Carter, A., Baudraz, V. (2004): Miocene to Holocene exhumation of metamorphic crustal wedges in the Himalayan orogen: evidence for tectonic extrusion coupled to fluvial erosion. *Tectonics*, **23**, article No TC1014.

van den Kerkhof, A.M. & Hein, U.F. (2001): Fluid inclusion petrography. *Lithos*, **55**, 27-47.

Visonà, D. & Lombardo, B. (2002): Two mica- and tourmaline leucogranites from the Everest- Makalu region (Nepal-Tibet): Himalayan leucogranite genesis by isobaric heating? *Lithos*, **62**, 125-150.

Visonà, D., Villa, I.M., Pertusati, P., Lombardo, B. (2000): Different varieties of Miocene leucogranite in the Arun Valley– Everest-Makalu area: field relations, petrology and isotope geochemistry. Earth Science Frontiers, 15th Himalaya-Karakorum-Tibet International Workshop, Abstract Volume, China University of Geosciences, Beijing, 100-101.

Winslow, D.M., Zeitler, P.K., Chamberlain, C.P., Hollister, L.S. (1994): Direct evidence for a steep geotherm under conditions of rapid denudation, Western Himalaya, Pakistan. *Geology*, **22**, 1075-1078.

Yardley, B., Gleeson, S., Bruce, S., Banks, D. (2000): Origin of retrograde fluids in metamorphic rocks. *J. Geochem. Explor.*, **69-70**, 281-285.

Yin, C., & Kuo, S.T. (1978): Stratigraphy of the Mount Jolmo Lungma and its North slope. *Scientia Sinica*, **21**, 629-644.

Zakrutkin, V.V. (1968): The evolution of amphiboles during metamorphism. *Zapiski Vsesoyuznovo Mineralogicheskovo Obshchestva*, **96**, 13-23.

Zhang, J., & Guo, L. (2007): Structure and geochronology of the southern Xainza-Dinggye rift and its relationship to the south Tibetan detachment system. *J. Asian Earth Sci.,* **29,** 722-736.

Received 3 November 2006
Modified version received 20 April 2007
Accepted 24 Mai 2007